

Measurement of prompt J/ψ and beauty hadron production cross sections at mid-rapidity in pp collisions at $\sqrt{s} = 7$ TeV

**ALICE****The ALICE Collaboration***E-mail:* Giuseppe.Bruno@ba.infn.it

ABSTRACT: The ALICE experiment at the LHC has studied J/ψ production at mid-rapidity in pp collisions at $\sqrt{s} = 7$ TeV through its electron pair decay on a data sample corresponding to an integrated luminosity $L_{\text{int}} = 5.6 \text{ nb}^{-1}$. The fraction of J/ψ from the decay of long-lived beauty hadrons was determined for J/ψ candidates with transverse momentum $p_t > 1.3 \text{ GeV}/c$ and rapidity $|y| < 0.9$. The cross section for prompt J/ψ mesons, i.e. directly produced J/ψ and prompt decays of heavier charmonium states such as the $\psi(2S)$ and χ_c resonances, is $\sigma_{\text{prompt } J/\psi}(p_t > 1.3 \text{ GeV}/c, |y| < 0.9) = 8.3 \pm 0.8 \text{ (stat.)} \pm 1.1 \text{ (syst.)} {}^{+1.5}_{-1.4} \text{ (syst. pol.)} \mu\text{b}$. The cross section for the production of b-hadrons decaying to J/ψ with $p_t > 1.3 \text{ GeV}/c$ and $|y| < 0.9$ is $\sigma_{J/\psi \leftarrow \text{hB}}(p_t > 1.3 \text{ GeV}/c, |y| < 0.9) = 1.46 \pm 0.38 \text{ (stat.)} {}^{+0.26}_{-0.32} \text{ (syst.)} \mu\text{b}$. The results are compared to QCD model predictions. The shape of the p_t and y distributions of b-quarks predicted by perturbative QCD model calculations are used to extrapolate the measured cross section to derive the $b\bar{b}$ pair total cross section and $d\sigma/dy$ at mid-rapidity.

KEYWORDS: Hadron-Hadron ScatteringARXIV EPRINT: [1205.5880](https://arxiv.org/abs/1205.5880)

Contents

1	Introduction	1
2	Experiment and data analysis	2
3	Systematic uncertainties	6
4	Results	10
4.1	Fraction of J/ψ from the decay of b-hadrons	10
4.2	Prompt J/ψ production	11
4.3	Beauty hadron production	13
5	Summary	16
	The ALICE collaboration	22

1 Introduction

The production of both charmonium mesons and beauty-flavoured hadrons, referred to as b-hadrons or h_B in this paper, in hadronic interactions represents a challenging testing ground for models based on Quantum ChromoDynamics (QCD).

The mechanisms of J/ψ production operate at the boundary of the perturbative and non-perturbative regimes of QCD. At hadron colliders, J/ψ production was extensively studied at the Tevatron [1–4] and RHIC [5]. Measurements in the new energy domain of the Large Hadron Collider (LHC) can contribute to a deeper understanding of the physics of the hadroproduction processes. The first LHC experimental results on the J/ψ transverse momentum (p_t) differential cross sections [6–10] are well described by various theoretical approaches [11–14]. Among those results, the ALICE Collaboration reported the measurement of the rapidity (y) and transverse momentum dependence of inclusive J/ψ production in proton–proton (pp) collisions at $\sqrt{s} = 7$ TeV [9]. The inclusive J/ψ yield is composed of three contributions: prompt J/ψ produced directly in the proton–proton collision, prompt J/ψ produced indirectly (via the decay of heavier charmonium states such as χ_c and $\psi(2S)$), and non-prompt J/ψ from the decay of b-hadrons. Other LHC experiments have separated the prompt and non-prompt J/ψ component [6–8, 10]. However, at mid-rapidity, only the high- p_t part of the differential $d\sigma_{J/\psi}/dp_t$ distribution was measured ($p_t > 6.5$ GeV/ c), i.e. a small fraction (few percent) of the p_t -integrated cross section.

The measurement of the production of b-hadrons in pp collisions at the LHC provides a way to test, in a new energy domain, calculations of QCD processes based on the factorization approach. In this scheme, the cross sections are computed as a convolution of the

parton distribution functions of the incoming protons, the partonic hard scattering cross sections, and the fragmentation functions. Measurements of cross sections for beauty quark production in high-energy hadronic interactions have been done in the past at $p\bar{p}$ colliders at center-of-mass energies from 630 GeV [15, 16] to 1.96 TeV [2, 17–19] and in p-nucleus collisions with beam energies from 800 to 920 GeV [20]. The LHC experiments have reported measurements of b-hadron production in pp collisions at $\sqrt{s} = 7$ TeV by studying either exclusive decays of B mesons [21–23] or semi-inclusive decays of b-hadrons [6–8, 10, 24, 25]. At mid-rapidity, the measurements are available only for p_t of the b-hadrons larger than ≈ 5 GeV/c, whereas the low p_t region of the differential b-hadron cross sections, where the bulk of the b-hadrons is produced, has not been studied.

In this paper, the fraction of J/ψ from the decay of b-hadrons in pp collisions at $\sqrt{s} = 7$ TeV for J/ψ in the ranges $1.3 < p_t < 10$ GeV/c and $|y| < 0.9$ is determined. This information is combined with the previous inclusive J/ψ cross section measurement reported by ALICE [9]. Prompt J/ψ and b-hadron cross sections are thus determined at mid-rapidity down to the lowest p_t reach at the LHC energy.

2 Experiment and data analysis

The ALICE experiment [26] consists of a central barrel, covering the pseudorapidity region $|\eta| < 0.9$, and a muon spectrometer with $-4 < \eta < -2.5$ coverage. The results presented in this paper were obtained with the central barrel tracking detectors, in particular the Inner Tracking System (ITS) [26, 27] and the Time Projection Chamber (TPC) [28]. The ITS, which consists of two innermost Silicon Pixel Detector (SPD), two Silicon Drift Detector (SDD), and two outer Silicon Strip Detector (SSD) layers, provides up to six space points (hits) for each track. The TPC is a large cylindrical drift detector with an active volume that extends over the ranges $85 < r < 247$ cm and $-250 < z < 250$ cm in the radial and longitudinal (beam) directions, respectively. The TPC provides up to 159 space points per track and charged particle identification via specific energy loss (dE/dx) measurement.

The event sample, corresponding to 3.5×10^8 minimum bias events and an integrated luminosity $L_{\text{int}} = 5.6 \text{ nb}^{-1}$, event selection and track quality cuts used for the measurement of the inclusive J/ψ production at mid-rapidity [9] were also adopted in this analysis. In particular, an event with a reconstructed vertex position z_v was accepted if $|z_v| < 10$ cm. The tracks were required to have a minimum p_t of 1 GeV/c, a minimum number of 70 TPC space points, a χ^2 per space point of the momentum fit lower than 4, and to point back to the interaction vertex within 1 cm in the transverse plane. At least one hit in either of the two layers of the SPD was required. For tracks passing this selection, the average number of hits in the six ITS layers was 4.5–4.7, depending on the data taking period. The electron identification was based on the specific energy loss in the TPC: a $\pm 3\sigma$ inclusion cut around the Bethe-Bloch fit for electrons and $\pm 3.5\sigma$ ($\pm 3\sigma$) exclusion cut for pions (protons) were employed [9]. Finally, electron or positron candidates compatible, together with an opposite charge candidate, with being products of γ conversions (the invariant mass of the pair being smaller than $100 \text{ MeV}/c^2$) were removed, in order to reduce the combinatorial background. It was verified, using a Monte Carlo simulation, that this procedure does

not affect the J/ψ signal. In this analysis, opposite-sign (OS) electron pairs were divided in three “types”: type “first-first” (FF) corresponds to the case when both the electron and the positron have hits in the first pixel layer, type “first-second” (FS) are those pairs where one of them has a hit in the first layer and the other does not, while for the type “second-second” (SS) neither of them has a hit in the first layer. The candidates of type SS , which correspond to about 10% of the total, were discarded due to the worse spatial resolution of the associated decay vertex.

A detailed description of the track and vertex reconstruction procedures can be found in [29]. The primary vertex was determined via an analytic χ^2 minimization method in which tracks are approximated as straight lines after propagation to their common point of closest approach. The vertex fit was constrained in the transverse plane using the information on the position and spread of the luminous region. The latter was determined from the distribution of primary vertices reconstructed over the run. Typically, the transverse position of the vertex has a resolution that ranges from 40 μm in low-multiplicity events with less than 10 charged particles per unit of rapidity to about 10 μm in events with a multiplicity of about 40. For each J/ψ candidate a specific primary vertex was also calculated by excluding the J/ψ decay tracks, in order to estimate a systematic uncertainty related to the evaluation of the primary vertex in the case of events with non-prompt J/ψ , as discussed in section 3. The decay vertex of the J/ψ candidate was computed with the same analytic χ^2 minimization as for the primary vertex, using the two decay tracks only and without the constraint of the luminous region.

The measurement of the fraction of the J/ψ yield coming from b-hadron decays, f_B , relies on the discrimination of J/ψ mesons produced at a distance from the pp collision vertex. The signed projection of the J/ψ flight distance onto its transverse momentum vector, $\vec{p}_t^{J/\psi}$, was constructed according to the formula

$$L_{xy} = \vec{L} \cdot \vec{p}_t^{J/\psi} / p_t^{J/\psi}, \quad (2.1)$$

where \vec{L} is the vector from the primary vertex to the J/ψ decay vertex. The variable x , referred to as “pseudoproper decay length” in the following, was introduced to separate prompt J/ψ from those produced by the decay of b-hadrons,¹

$$x = \frac{c \cdot L_{xy} \cdot m_{J/\psi}}{p_t^{J/\psi}}, \quad (2.2)$$

where $m_{J/\psi}$ is the (world average) J/ψ mass [30].

For events with very low J/ψ p_t , the non-negligible amount of J/ψ with large opening angle between its flight direction and that of the b-hadron impairs the separation ability. Monte Carlo simulation shows that the detector resolution allows the determination of the fraction of J/ψ from the decay of b-hadrons for events with J/ψ p_t greater than 1.3 GeV/c.

An unbinned 2-dimensional likelihood fit was used to determine the ratio of the non-prompt to inclusive J/ψ production and the ratio of J/ψ signal candidates (the sum of

¹The variable x , which was introduced in [1], mimics a similar variable used for b-hadron lifetime measurements where b-hadrons are reconstructed exclusively and therefore the mass and p_t of the b-hadron can be used in place of those of the J/ψ , to get $c\tau = \frac{L}{\beta\gamma} = \frac{c \cdot L_{xy} \cdot M_{\text{b-hadron}}}{p_t^{\text{b-hadron}}}$.

both prompt and non-prompt components) to the total number of candidates, f_{Sig} , by maximizing the quantity

$$\ln L = \sum_{i=1}^N \ln F(x, m_{e^+e^-}), \quad (2.3)$$

where $m_{e^+e^-}$ is the invariant mass of the electron pair and N is the total number of candidates in the range $2.4 < m_{e^+e^-} < 4.0 \text{ GeV}/c^2$. The expression for $F(x, m_{e^+e^-})$ is

$$F(x, m_{e^+e^-}) = f_{\text{Sig}} \cdot F_{\text{Sig}}(x) \cdot M_{\text{Sig}}(m_{e^+e^-}) + (1 - f_{\text{Sig}}) \cdot F_{\text{Bkg}}(x) \cdot M_{\text{Bkg}}(m_{e^+e^-}), \quad (2.4)$$

where $F_{\text{Sig}}(x)$ and $F_{\text{Bkg}}(x)$ are Probability Density Functions (PDFs) describing the pseudoproper decay length distribution for signal and background candidates, respectively. $M_{\text{Sig}}(m_{e^+e^-})$ and $M_{\text{Bkg}}(m_{e^+e^-})$ are the PDFs describing the dielectron invariant mass distributions for the signal and background, respectively. A Crystal Ball function [31] is used for the former and an exponential function for the latter. The signal PDF is given by

$$F_{\text{Sig}}(x) = f'_B \cdot F_B(x) + (1 - f'_B) \cdot F_{\text{prompt}}(x), \quad (2.5)$$

where $F_{\text{prompt}}(x)$ and $F_B(x)$ are the PDFs for prompt and non-prompt J/ψ , respectively, and f'_B is the fraction of reconstructed non-prompt J/ψ ,

$$f'_B = \frac{N_{J/\psi \leftarrow \text{hB}}}{N_{J/\psi \leftarrow \text{hB}} + N_{\text{prompt } J/\psi}}, \quad (2.6)$$

which can differ (see below) from f_B due to different acceptance and reconstruction efficiency of prompt and non-prompt J/ψ . The distribution of non-prompt J/ψ is the convolution of the x distribution of J/ψ from b-hadron events, $\chi_B(x)$, and the experimental resolution on x , $R_{\text{type}}(x)$, which depends on the type of candidate (FF or FS),

$$F_B(x) = \chi_B(x') \otimes R_{\text{type}}(x' - x). \quad (2.7)$$

Promptly produced J/ψ mesons decay at the primary vertex, and their pseudoproper decay length distribution is thus simply described by $R_{\text{type}}(x)$:

$$F_{\text{prompt}}(x) = \delta(x') \otimes R_{\text{type}}(x' - x) = R_{\text{type}}(x). \quad (2.8)$$

The resolution function is described by the sum of two Gaussians and a power law function reflected about $x = 0$ and was determined, as a function of the p_t of the J/ψ , with a Monte Carlo simulation study. In this simulation, which utilizes GEANT3 [32] and incorporates a detailed description of the detector material, geometry, and response, prompt J/ψ were generated with a p_t distribution extrapolated from CDF measurements [1] and a y distribution parameterization taken from Color Evaporation Model (CEM) calculations [33]. These J/ψ were individually injected into proton–proton collisions simulated using the PYTHIA 6.4.21 event generator [34, 35], and reconstructed as for J/ψ candidates in data. A data-driven method (discussed in section 3) was also developed and used to estimate the systematic uncertainty related to this procedure. The Monte Carlo x distribution of J/ψ from the decay of b-hadrons produced in proton-proton collisions simulated

using the PYTHIA 6.4.21 event generator [34, 35] with Perugia-0 tuning [36] was taken as the template for the x distribution of b-hadron events in data, $\chi_B(x)$. A second template, used to estimate the systematic uncertainty, was obtained by decaying the simulated b-hadrons using the EvtGen package [37], and describing the final state radiation (“internal” bremsstrahlung) using PHOTOS [38, 39].

For the background x distribution, $F_{\text{Bkg}}(x)$, the functional form employed by CDF [1] was used,

$$F_{\text{Bkg}}(x) = (1 - f_+ - f_- - f_{\text{sym}})R_{\text{type}}(x) + \left[\frac{f_+}{\lambda_+} e^{-x'/\lambda_+} \theta(x') + \frac{f_-}{\lambda_-} e^{x'/\lambda_-} \theta(-x') + \frac{f_{\text{sym}}}{2\lambda_{\text{sym}}} e^{-|x'|/\lambda_{\text{sym}}} \right] \otimes R_{\text{type}}(x' - x), \quad (2.9)$$

where $\theta(x)$ is the step function, f_+ , f_- and f_{sym} are the fractions of three components with positive, negative and symmetric decay length exponential distributions, respectively. The effective parameters λ_+ , λ_- and λ_{sym} , and optionally also the corresponding fractions, were determined, prior to the likelihood fit maximization, with a fit to the x distribution in the sidebands of the dielectron invariant mass distribution, defined as the regions 1.8–2.6 and 3.2–5.0 GeV/ c^2 . The introduction of these components is needed because the background consists also of random combinations of electrons from semi-leptonic decays of charm and beauty hadrons, which tend to produce positive x values, as well as of other secondary or mis-reconstructed tracks which contribute both to positive and negative x values. The first term in eq. (2.9), proportional to $R_{\text{type}}(x)$, describes the residual combinatorics of primary particles.

In figure 1 the distributions of the invariant mass and the pseudoproper decay length, the latter restricted to candidates with $2.92 < m_{e^+e^-} < 3.16$ GeV/ c^2 , for opposite-sign electron pairs with $p_t > 1.3$ GeV/ c are shown with superimposed projections of the maximum likelihood fit result.

The value of the fit parameter f'_B provides the fraction of non-prompt J/ ψ which were reconstructed. In principle prompt and non-prompt J/ ψ can have different acceptance times efficiency ($A \times \epsilon$) values. This can happen because of two effects: (i) the $A \times \epsilon$ depends on the p_t of the J/ ψ and prompt and non-prompt J/ ψ have different p_t distributions within the considered p_t range; (ii) at a given p_t , prompt and non-prompt J/ ψ can have different polarization and, therefore, a different acceptance. The fraction of non-prompt J/ ψ , corrected for these effects, was obtained as

$$f_B = \left(1 + \frac{1 - f'_B}{f'_B} \cdot \frac{\langle A \times \epsilon \rangle_B}{\langle A \times \epsilon \rangle_{\text{prompt}}} \right)^{-1}, \quad (2.10)$$

where $\langle A \times \epsilon \rangle_B$ and $\langle A \times \epsilon \rangle_{\text{prompt}}$ are the average acceptance times efficiency values, in the considered p_t range and for the assumed polarization state, of non-prompt and prompt J/ ψ , respectively. The acceptance times efficiency ($A \times \epsilon$) varies very smoothly with p_t and, for unpolarized J/ ψ in the p_t range from 1.3 to 10 GeV/ c , has a minimum of 8% at 2 GeV/ c and a broad maximum of 12% at 7 GeV/ c [9]. As a consequence, the $\langle A \times \epsilon \rangle$ values of prompt and non-prompt J/ ψ differ by about 3% only in this integrated p_t range.

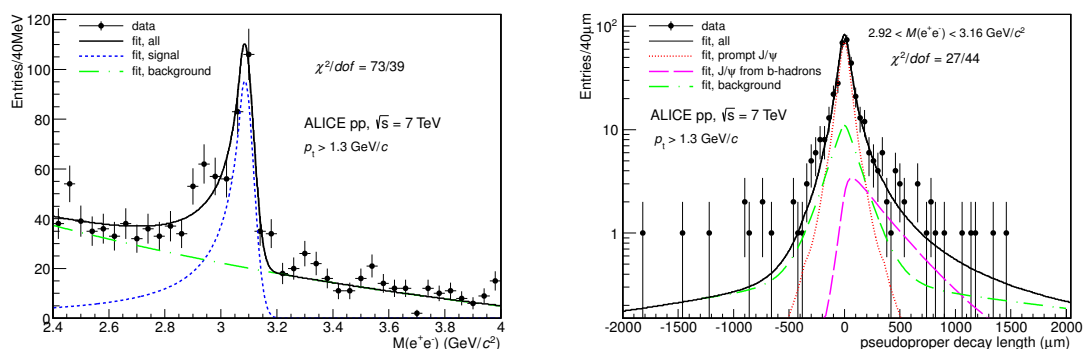


Figure 1. Invariant mass (left panel) and pseudoproper decay length (right panel) distributions of opposite sign electron pairs for $|y_{J/\psi}| < 0.9$ and $p_t^{J/\psi} > 1.3 \text{ GeV}/c$ with superimposed projections of the maximum likelihood fit. The latter distribution is limited to the J/ψ candidates under the mass peak, i.e. for $2.92 < m_{e^+e^-} < 3.16 \text{ GeV}/c^2$, for display purposes only. The χ^2 values of these projections are reported for both distributions.

The central values of the resulting cross sections are quoted assuming both prompt and non-prompt J/ψ to be unpolarized and the variations due to different assumptions are estimated as a separate systematic uncertainty. The polarization of J/ψ from b-hadron decays is expected to be much smaller than for prompt J/ψ due to the averaging effect caused by the admixture of various exclusive $B \rightarrow J/\psi + X$ decay channels. In fact, the sizeable polarization, which is observed when the polarization axis refers to the B-meson direction [40], is strongly smeared when calculated with respect to the direction of the daughter J/ψ [7], as indeed observed by CDF [2]. Therefore, these variations will be calculated in the two cases of prompt J/ψ with fully transverse ($\lambda = 1$) or longitudinal ($\lambda = -1$) polarization, in the Collins-Soper (CS) and helicity (HE) reference frames,² the non-prompt component being left unpolarized.

Despite the small J/ψ candidate yield, amounting to about 400 counts, the data sample could be divided into four p_t bins (1.3–3, 3–5, 5–7 and 7–10 GeV/c), and the fraction f_B was evaluated in each of them with the same technique. At low p_t the statistics is higher, but the resolution is worse and the signal over background, S/B , is smaller (i.e. f_{Sig} is smaller). At high p_t the statistics is smaller, but the resolution improves and the background becomes negligible. In figure 2 the distributions of the invariant mass and of the pseudoproper decay length are shown in different p_t bins with superimposed results of the fits.

3 Systematic uncertainties

The different contributions to the systematic uncertainties affecting the measurement of the fraction of J/ψ from the decay of b-hadrons are discussed in the following, referring to the integrated p_t range, and summarized in table 1.

²The polar angle distribution of the J/ψ decay leptons is given by $dN/d \cos \theta = 1 + \lambda \cos^2 \theta$.

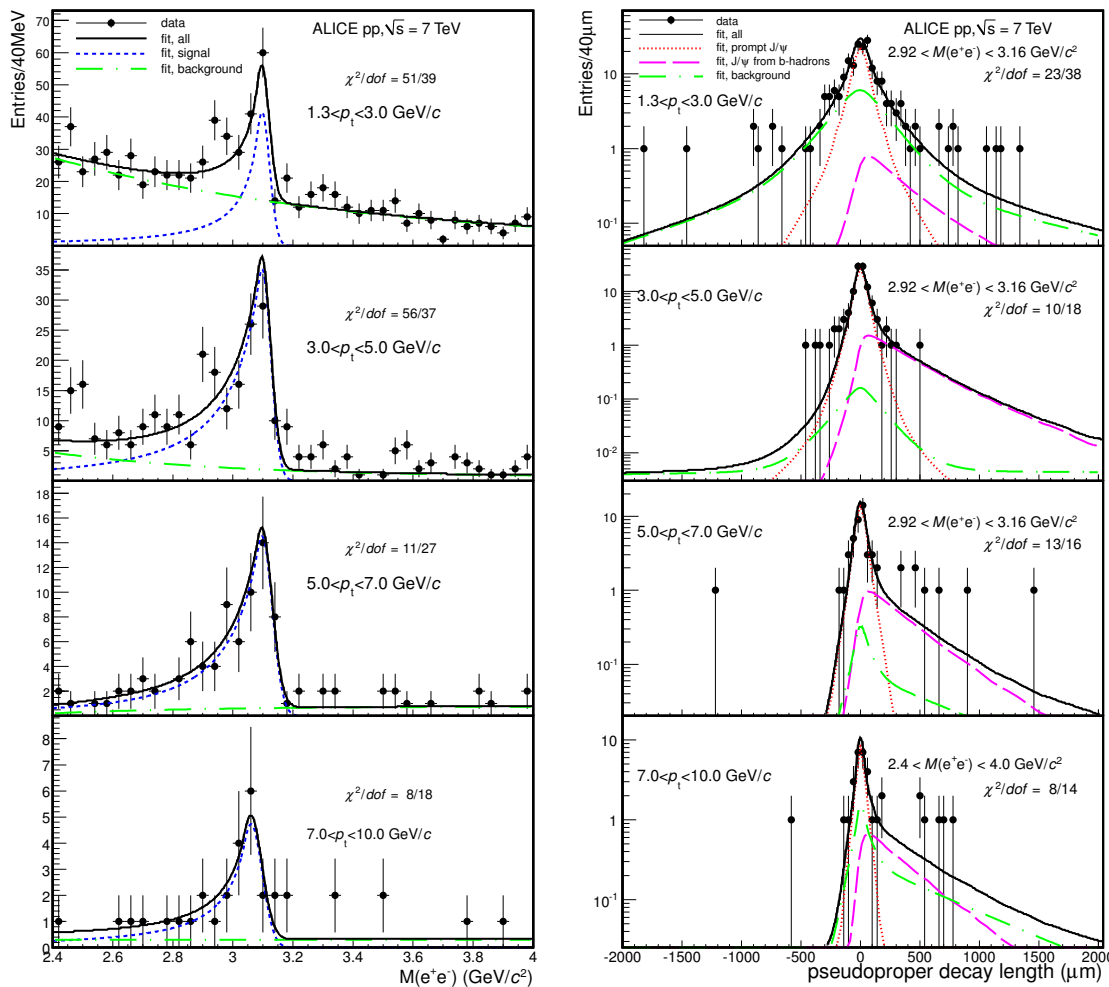


Figure 2. Invariant mass (left panels) and pseudoproper decay length (right panels) distributions of opposite sign electron pairs in different p_t bins with superimposed projections of the maximum likelihood fit. The χ^2 values of these projections are also reported for all distributions.

- *Resolution function.* The resolution function was determined from a Monte Carlo simulation, as discussed above. The fits were repeated by artificially modifying the resolution function, according to the formula

$$R'_{\text{type}}(x) = \frac{1}{1 + \delta} R_{\text{type}}\left(\frac{x}{1 + \delta}\right),$$

where δ is a constant representing the desired relative variation of the RMS of the resolution function. Studies on track distance of closest approach to the primary interaction vertex in the bending plane (d_0) show that the p_t dependence of the d_0 resolution as measured in the data is reproduced within about 10% by the Monte Carlo simulation [29], but with a systematically worse resolution in data. For the x variable a similar direct comparison to data is not straightforward, however, the residual discrepancy is not expected to be larger than that observed for d_0 .

The variations of f_B obtained in the likelihood fit results by varying δ from -5% to $+10\%$ are $+8\%$ and -15% , respectively, and they were assumed as the systematic uncertainty due to this contribution.

An alternative, data-driven, approach was also considered. The x distribution of the signal, composed of prompt and non-prompt J/ψ , was obtained by subtracting the x distribution of the background, measured in the sidebands of the invariant mass distribution. This distribution is then fitted by fixing the ratio of prompt to non-prompt J/ψ to that obtained from the likelihood fit and leaving free the parameters of the resolution function. The RMS of the fitted resolution function is found to be 8% larger than the one determined using the Monte Carlo simulation, hence within the range of variation assumed for δ .

- *Pseudoproper decay length distribution of background.* The shape of the combinatorial background was determined from a fit to the x distribution of candidates in the sidebands of the invariant mass distribution. By varying the fit parameters within their errors an envelope of distributions was obtained, whose extremes were used in the likelihood fit in place of the most probable distribution. The variations in the result of the fit were determined and adopted as systematic uncertainties. Also, it was verified that the x distribution obtained for like-sign (LS) candidates, with invariant mass in the range from 2.92 to $3.16 \text{ GeV}/c^2$ complementary to the sidebands, is best fitted by a distribution which falls within the envelope of the OS distributions. Finally, the likelihood fit was repeated by relaxing, one at a time, the parameters of the functional form (eq. (2.9)) and it was found that the values of f_B were within the estimated uncertainties. The estimated systematic uncertainty is 6% .
- *Pseudoproper decay length distribution of b -hadrons.* The fits were also done using as template for the x distribution of b -hadrons, $\chi_B(x)$, that obtained by the EvtGen package [37], and describing the final state radiation using PHOTOS [38, 39]. The central values of the fits differ by a few percent at most and the resulting systematic uncertainty is 3% .
- *Invariant mass distributions.* The likelihood method was used in this analysis to fit simultaneously the invariant mass distribution, which is sensitive to the ratio of signal to all candidates (f_{Sig}), and the x distribution, which determines the ratio of non-prompt to signal candidates (f_B). The statistical uncertainties on these quantities were therefore evaluated together, including the effects of correlations. However, the choice of the function describing the invariant mass distribution, as well as the procedure, can introduce systematic uncertainties in the evaluation of f_B . Different approaches were therefore considered: (i) the functional form describing the background was changed into an exponential plus a constant and the fit repeated; (ii) the background was described using the LS distribution and the signal was obtained by subtracting the LS from the OS distributions. The signal and the background shapes were determined with χ^2 minimizations. Both functional forms, exponential and exponential plus a constant, were considered for the background. The likelihood

fit was then performed again to determine f_B (and f_{Sig}); (iii) the same procedure as in (ii) was used, but additionally f_{Sig} was estimated *a priori* using a bin counting method [9] instead of the integrals of the best fit functions. The maximum likelihood fit was performed with f_{Sig} fixed to this new value; (iv) and (v) the same procedures as in (ii) and (iii) were used but with the background described by a track rotation (TR) method [9].

Half of the difference between the maximum and minimum f_B values obtained with the different methods was assumed as systematic uncertainty. It amounts to about 6%.

- *Primary vertex.* The effect of excluding the decay tracks of the J/ψ candidate in the computation of the primary vertex was studied with the Monte Carlo simulation: on the one hand, for the prompt J/ψ , the x resolution function is degraded, due to the fact that two prompt tracks are not used in the computation of the vertex, which is thus determined with less accuracy. The effect on the resolution is p_t dependent, with the RMS of the x distribution of prompt J/ψ increasing by 15% at low p_t and by 7% at high p_t . On the other hand, for non-prompt J/ψ a bias on the x determination should be reduced. The bias consists in an average shift of the primary vertex towards the secondary decay vertex of the b-hadrons, which is reflected in a shift of the mean of the x distribution by about $4 \mu\text{m}$ for the p_t -integrated distribution. However, the shift is p_t and “type” dependent. In some cases the bias is observed in the opposite direction and is enhanced by removing the decay tracks of the candidate. This can happen since b-quarks are always produced in pairs. If a charged track from the fragmentation of the second b-quark also enters the acceptance, it can pull the primary vertex position towards the opposite direction. In the end, therefore, the primary vertex was computed without removing the decay tracks of the candidates. To estimate the systematic uncertainty, the analysis was repeated by either (i) removing the decay tracks in the computation of the primary vertex and using the corresponding worse resolution function in the fit or (ii) keeping those tracks and introducing an *ad hoc* shift in the distribution of the $\chi_B(x)$, equal to that observed in the Monte Carlo simulation for non-prompt J/ψ . The contribution to the systematic uncertainty is about 5%.
- *MC p_t spectrum.* The ratio $\frac{\langle A \times \epsilon \rangle_B}{\langle A \times \epsilon \rangle_{\text{prompt}}}$ in eq. (2.10) was computed using MC simulations: prompt J/ψ were generated with the p_t distribution extrapolated from CDF measurements [1] and the y distribution parameterized from CEM [33]; b-hadrons were generated using the PYTHIA 6.4.21 [34, 35] event generator with Perugia-0 tuning [36]. By varying the average p_t of the J/ψ distributions within a factor 2, a 1.5% variation in the acceptance was obtained both for prompt and non-prompt J/ψ . Such a small value is a consequence of the weak p_t dependence of the acceptance. For the measurement integrated over p_t ($p_t > 1.3 \text{ GeV}/c$), the $A \times \epsilon$ values of prompt and non-prompt J/ψ differ by about 3% only. The uncertainty due to Monte Carlo p_t distributions is thus estimated to be 1%. When estimating f_B in p_t bins, this uncertainty is negligible.

Source	Systematic uncertainty (%)		
	p_t integrated	lowest p_t bin	highest p_t bin
Resolution function	+8, -15	+15, -25	+2, -3
x distribution of background	± 6	± 13	± 1
x distribution of b-hadrons	± 3	± 3	± 2
$m_{e^+e^-}$ distributions	± 6	± 11	± 4
Primary vertex	+4, -5	± 4	+4, -8
MC p_t spectrum	± 1	0	0
Total	+12, -18	+23, -30	+6, -9
Polarization (prompt J/ψ)			
CS ($\lambda = -1$)	+13	+22	+5
CS ($\lambda = +1$)	-10	-19	-3
HE ($\lambda = -1$)	+17	+19	+11
HE ($\lambda = +1$)	-14	-16	-8

Table 1. Systematic uncertainties (in percent) on the measurement of the fraction of J/ψ from the decay of b-hadrons, f_B . The variations of f_B are also reported, with respect to the case of both prompt and non-prompt J/ψ unpolarized, when assuming the prompt component with given polarization.

- *Polarization.* The variations of f_B obtained assuming different polarization scenarios for the prompt component only were evaluated, as discussed in section 2, and are reported in table 1. The maximum variations are quoted as separate errors.

The study of systematic uncertainties was repeated as a function of p_t . In table 1 the results are summarized for the integrated p_t range ($p_t > 1.3 \text{ GeV}/c$) and for the lowest (1.3–3 GeV/c) and highest (7–10 GeV/c) p_t bins. All systematic uncertainties increase with decreasing p_t , except the one related to the primary vertex measurement.

4 Results

4.1 Fraction of J/ψ from the decay of b-hadrons

The fraction of J/ψ from the decay of b-hadrons in the experimentally accessible kinematic range, $p_t > 1.3 \text{ GeV}/c$ and $|y| < 0.9$, which is referred to as “measured region” in the following, is

$$f_B = 0.149 \pm 0.037 \text{ (stat.)}^{+0.018}_{-0.027} \text{ (syst.)}^{+0.025}_{-0.021} (\lambda_{\text{HE}}=1) (\lambda_{\text{HE}}=-1) \text{ (syst.pol.)}.$$

The fractions measured in the p_t bins are reported in table 2 and shown in figure 3. In the figure, the data symbols are placed at the average value of the p_t distribution of each bin. The average was computed using the above mentioned Monte Carlo distributions: the one based on the CDF extrapolation [33] and that using PYTHIA [34, 35] with Perugia-0 tuning [36] for prompt and non-prompt J/ψ , respectively, weighted by the measured f_B . In figure 3 the results of the ATLAS [8] and CMS [10] experiments measured at mid-rapidity

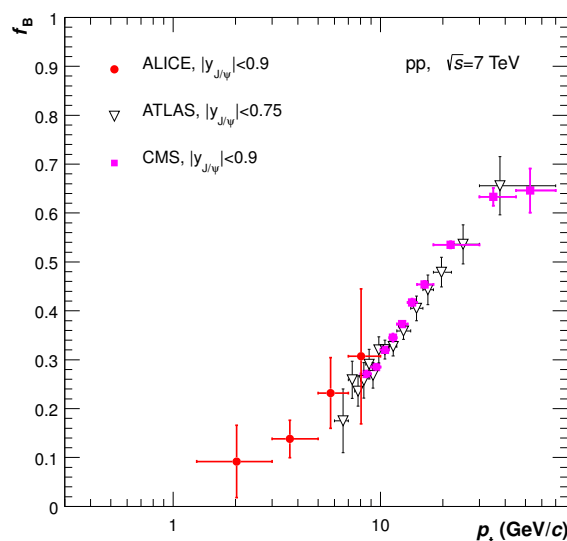


Figure 3. The fraction of J/ψ from the decay of b-hadrons as a function of p_t of J/ψ compared with results from ATLAS [8] and CMS [10] in pp collisions at $\sqrt{s} = 7$ TeV.

for the same colliding system are also shown. The ALICE results extend the mid-rapidity measurements down to low p_t .

4.2 Prompt J/ψ production

By combining the measurement of the inclusive J/ψ cross section, which was determined as described in [9], and the f_B value, the prompt J/ψ cross section was obtained:

$$\sigma_{\text{prompt } J/\psi} = (1 - f_B) \cdot \sigma_{J/\psi}. \quad (4.1)$$

The numerical values of the inclusive J/ψ cross section in the p_t ranges used for this analysis are summarized in table 2. In the measured region the integrated cross section is $\sigma_{\text{prompt } J/\psi}(|y| < 0.9, p_t > 1.3 \text{ GeV}/c) = 8.3 \pm 0.8(\text{stat.}) \pm 1.1(\text{syst.})^{+1.5(\lambda_{\text{HE}}=1)}_{-1.4(\lambda_{\text{HE}}=-1)} \mu\text{b}$. The systematic uncertainties related to the unknown polarization are quoted for the reference frame where they are the largest.

The differential distribution $\frac{d^2\sigma_{\text{prompt } J/\psi}}{dp_t dy}$ is shown as a function of p_t in figure 4 and $\frac{d\sigma_{\text{prompt } J/\psi}}{dy}$ is plotted in figure 5. The numerical values are summarized in table 2. In figure 4 the statistical and all systematic errors are added in quadrature for better visibility, while in figure 5 the error bar shows the quadratic sum of statistical and systematic errors, except for the 3.5% systematic uncertainty on luminosity and the 1% on the branching ratio (BR), which are added in quadrature and shown as box. The results shown in figures 4 and 5 assume unpolarized J/ψ production. Systematic uncertainties due to the unknown J/ψ polarization are not shown. Results by the CMS [6, 10], LHCb [7] and ATLAS [8] Collaborations are shown for comparison. Also for these data the uncertainties due to luminosity and to the BR are shown separately (boxes) in figure 5, while the error

p_t (GeV/c)	$\langle p_t \rangle$ (GeV/c)	Measured quantity	Systematic uncertainties				
			Correl.	Non-correl.	Extrap.	Polariz., CS	Polariz., HE
f_B (%)							
1.3–3.0	2.02	9.2 ± 7.4	0	+2.1, –2.8	0	+2.0, –1.7	+1.7, –1.5
3.0–5.0	3.65	13.8 ± 3.8	0	+1.5, –2.1	0	+1.3, –1.0	+2.1, –3.0
5.0–7.0	5.75	23.2 ± 7.2	0	+1.6, –2.1	0	+0.2, –0.2	+3.5, –2.6
7.0–10.0	8.06	30.7 ± 13.8	0	+1.8, –2.8	0	+1.5, –0.9	+3.4, –2.5
$p_t > 1.3$	2.85	14.9 ± 3.7	0	+1.8, –2.7	0	+1.9, –1.5	+2.5, –2.1
$p_t > 0$	2.41	14.3 ± 3.6	0	+1.8, –2.6	+0.2, –0.5	+2.4, –1.6	+2.5, –1.9
$d^2\sigma_{J/\psi}/dydp_t$ ($\frac{\text{nb}}{\text{GeV}/c}$)							
1.3–3.0	2.02	1780 ± 210	± 65	± 250	0	+400, –320	+330, –280
3.0–5.0	3.65	715 ± 125	± 25	± 90	0	+50, –60	+170, –90
5.0–7.0	5.74	405 ± 70	± 15	± 45	0	+1, –3	+50, –50
7.0–10.0	8.06	60 ± 25	± 2	± 12	0	+2, –3	+5, –6
$d^2\sigma_{\text{prompt } J/\psi}/dydp_t$ ($\frac{\text{nb}}{\text{GeV}/c}$)							
1.3–3.0	2.02	1600 ± 230	± 60	± 230	0	+400, –320	+330, –280
3.0–5.0	3.65	620 ± 110	± 20	± 80	0	+50, –60	+170, –90
5.0–7.0	5.74	310 ± 60	± 10	± 35	0	+1, –3	+50, –50
7.0–10.0	8.03	40 ± 18	± 1	± 8	0	+2, –3	+5, –6
$\sigma_{\text{prompt } J/\psi}(y_{J/\psi} < 0.9)$ (μb)							
$p_t > 1.3$	2.81	8.3 ± 0.8		± 1.1	0	+1.0, –1.2	+1.5, –1.4
$p_t > 0$	2.37	10.6 ± 1.1		± 1.6	+0.06, –0.02	+1.6, –1.7	+1.9, –1.8
$\sigma_{J/\psi \leftarrow \text{hB}}(y_{J/\psi} < 0.9)$ (μb)							
$p_t > 1.3$	3.07	1.46 ± 0.38		+0.26, –0.32	0	0	0
$p_t > 0$	2.62	1.77 ± 0.46		+0.32, –0.39	+0.02, –0.06	0	0
$d\sigma_{b\bar{b}}/dy _{ y <0.9}$ (μb)							
		43 ± 11		+9, –10	+0.6, –1.5	0	0
$\sigma_{b\bar{b}}$ (μb)							
		282 ± 74		+58, –68	+8, –7	0	0

Table 2. The fraction of J/ψ from the decay of b-hadrons and cross sections. Some of the contributions to the systematic uncertainty do not depend on p_t , thus affecting only the overall normalization, and they are separately quoted (correl.). The contributions which depend on p_t , even when they are correlated bin by bin, were included among the non-correlated systematic errors. The values of $\langle p_t \rangle$ were computed using Monte Carlo distributions (see text for details).

bars represent the statistical and the other sources of systematic uncertainties added in quadrature.

The ALICE $\frac{d^2\sigma_{\text{prompt } J/\psi}}{dydp_t}$ measurement at mid-rapidity (left panel of figure 4) is complementary to the data of CMS, available for $|y| < 0.9$ and $p_t > 8 \text{ GeV}/c$, and ATLAS, which covers the region $|y| < 0.75$ and $p_t > 7 \text{ GeV}/c$. In the right panel of figure 4, the ALICE results are compared to next-to-leading order (NLO) non-relativistic QCD (NRQCD) theoretical calculations by M. Butenschön and B.A. Kniehl [12] and Y.-Q. Ma et al. [13]. Both calculations include color-singlet (CS), color-octet (CO), and heavier charmonium feed-down contributions. For one of the two models (M. Butenschön and B.A. Kniehl) the

partial results with only the CS contribution are also shown. The comparison suggests that the CO processes are indispensable to describe the data also at low p_t . The results are also compared to the model of V.A. Saleev et al. [14], which includes the contribution of partonic sub-processes involving t-channel parton exchanges and provides a prediction down to $p_t = 0$.

The ALICE result for $\frac{d\sigma_{\text{prompt J}/\psi}}{dy}$ (figure 5), which equals

$$\frac{d\sigma_{\text{prompt J}/\psi}}{dy} = 5.89 \pm 0.60(\text{stat.})_{-0.90}^{+0.88}(\text{syst.})_{-0.01}^{+0.03}(\text{extr.})_{-0.99}^{+1.01(\lambda_{\text{HE}}=1)} \mu\text{b},$$

was obtained by subtracting from the inclusive J/ ψ cross section measured for $p_t > 0$ that of J/ ψ coming from b-hadron decays. The latter was determined, as discussed in the next section, by extrapolating the cross section from the measured region down to $p_t > 0$ using an implementation of pQCD calculations at fixed order with next-to leading-log resummation (FONLL) [41]. The extrapolation uncertainty is negligible with respect to the other systematic uncertainties. In figure 5 the CMS and LHCb results for the rapidity bins where the p_t coverage extends down to zero were selected. For CMS, the value for $1.6 < |y| < 2.4$ was obtained by integrating the published $d^2\sigma_{\text{prompt J}/\psi}/dp_t dy$ data [6]. The ALICE data point at mid-rapidity complements the other LHC measurements of prompt J/ ψ production cross section as a function of rapidity. It is worth noting that the uncertainties of the data sets of the three experiments are uncorrelated, except for that (negligible) of the BR , while within the same experiment most of the systematic uncertainties are correlated. The prediction of the model by V.A. Saleev et al. [14] at mid-rapidity provides $\frac{d\sigma_{\text{prompt J}/\psi}}{dy} = 7.8_{-4.5}^{+9.7} \mu\text{b}$, which, within the large band of theoretical uncertainties, is in agreement with our measurement.

4.3 Beauty hadron production

The production cross section of J/ ψ from b-hadron decays was obtained as $\sigma_{\text{J}/\psi \leftarrow \text{h}_B} = f_B \cdot \sigma_{\text{J}/\psi}$. In the measured region it is

$$\sigma_{\text{J}/\psi \leftarrow \text{h}_B}(p_t > 1.3 \text{ GeV}/c, |y| < 0.9) = 1.46 \pm 0.38(\text{stat.})_{-0.32}^{+0.26}(\text{syst.}) \mu\text{b}.$$

This measurement can be compared to theoretical calculations based on the factorization approach. In particular, the prediction of the FONLL [41], which describes well the beauty production at Tevatron energy, provides [42] $1.33_{-0.48}^{+0.59} \mu\text{b}$, in good agreement with the measurement. For this calculation CTEQ6.6 parton distribution functions [43] were used and the theoretical uncertainty was obtained by varying the factorization and renormalization scales, μ_F and μ_R , independently in the ranges $0.5 < \mu_F/m_t < 2$, $0.5 < \mu_R/m_t < 2$, with the constraint $0.5 < \mu_F/\mu_R < 2$, where $m_t = \sqrt{p_t^2 + m_b^2}$. The beauty quark mass was varied within $4.5 < m_b < 5.0 \text{ GeV}/c^2$.

The same FONLL calculations were used to extrapolate the cross section of non-prompt J/ ψ down to p_t equal to zero. The extrapolation factor, which is equal to $1.212_{-0.038}^{+0.016}$, was computed as the ratio of the cross section for $p_t^{\text{J}/\psi} > 0$ and $|y_{\text{J}/\psi}| < 0.9$ to that in the measured region ($p_t^{\text{J}/\psi} > 1.3 \text{ GeV}/c$ and $|y_{\text{J}/\psi}| < 0.9$). Using the PYTHIA event generator

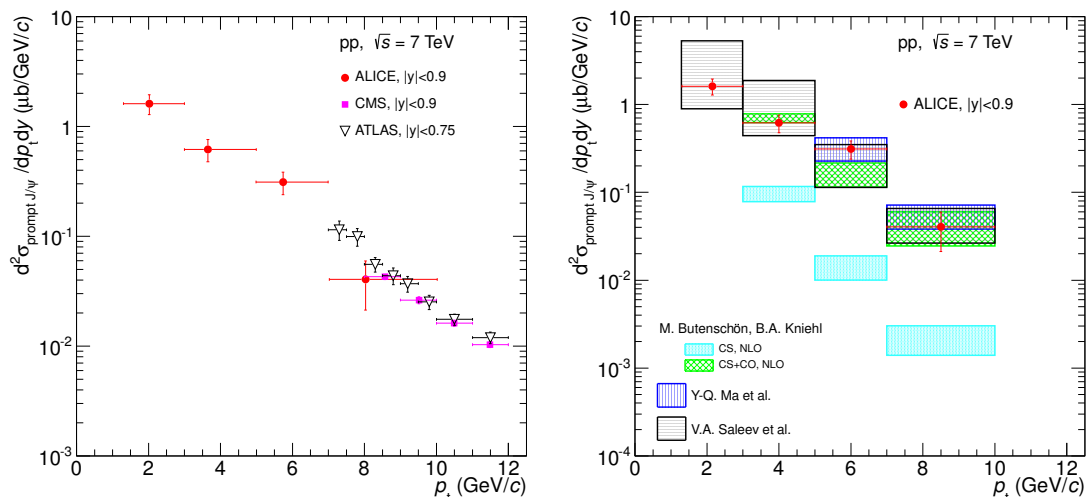


Figure 4. Double differential production cross section of prompt J/ψ as a function of p_t compared to results from ATLAS [8] and CMS [10] at mid-rapidity (left panel) and to theoretical calculations [12–14] (right panel). The error bars represent the quadratic sum of the statistical and systematic uncertainties.

with Perugia-0 tuning instead of FONLL provides an extrapolation factor of 1.156. The measured cross section corresponds thus to about 80% of the p_t -integrated cross section at mid-rapidity. Dividing by the rapidity range $\Delta y = 1.8$ one obtains

$$\frac{d\sigma_{J/\psi \leftarrow h_B}}{dy} = 0.98 \pm 0.26 \text{ (stat.)}_{-0.22}^{+0.18} \text{ (syst.)}_{-0.03}^{+0.01} \text{ (extr.) } \mu\text{b.}$$

In figure 6 this measurement is plotted together with the LHCb [7] and CMS [6] data at forward rapidity. For CMS the values for $1.2 < |y| < 1.6$ and $1.6 < |y| < 2.4$ were obtained by integrating the published $d^2\sigma_{J/\psi \leftarrow h_B}/dp_t dy$ data [6]; the value for $1.2 < |y| < 1.6$ was also extrapolated from $p_t^{\min} = 2.0 \text{ GeV}/c$ to $p_t = 0$, with the approach based on the FONLL calculations as previously described. The extrapolation uncertainties are shown in figure 6 as the slashed areas. The central FONLL prediction and its uncertainty band are also shown. A good agreement between data and theory is observed.

A similar procedure was used to derive the $b\bar{b}$ quark-pair production cross section

$$\frac{d\sigma_{b\bar{b}}}{dy} = \frac{d\sigma_{b\bar{b}}^{\text{theory}}}{dy} \times \frac{\sigma_{J/\psi \leftarrow h_B}(p_t^{J/\psi} > 1.3 \text{ GeV}/c, |y_{J/\psi}| < 0.9)}{\sigma_{J/\psi \leftarrow h_B}^{\text{theory}}(p_t^{J/\psi} > 1.3 \text{ GeV}/c, |y_{J/\psi}| < 0.9)}, \quad (4.2)$$

where the average branching fraction of inclusive b-hadron decays to J/ψ measured at LEP [44–46], $BR(h_b \rightarrow J/\psi + X) = (1.16 \pm 0.10)\%$, was used in the computation of $\sigma_{J/\psi \leftarrow h_B}^{\text{theory}}$. The extrapolation with the FONLL calculations provides

$$\frac{d\sigma_{b\bar{b}}}{dy} = 43 \pm 11 \text{ (stat.)}_{-10}^{+9} \text{ (syst.)}_{-1.5}^{+0.6} \text{ (extr.) } \mu\text{b.}$$

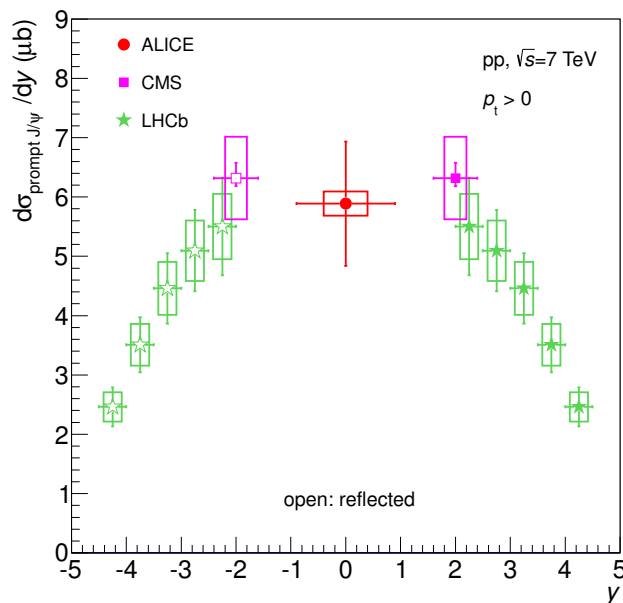


Figure 5. Prompt J/ψ production cross section as a function of rapidity. The error bars represent the quadratic sum of the statistical and systematic errors, while the systematic uncertainties on luminosity and branching ratio are shown as boxes around the data points. The symbols are plotted at the center of each bin. The CMS value was obtained by integrating the published $d^2\sigma_{\text{prompt } J/\psi}/dp_t dy$ data measured for $1.6 < |y| < 2.4$ [6]. The results obtained by LHCb [7] and CMS are reflected with respect to $y = 0$ (open symbols).

Using the PYTHIA event generator with Perugia-0 tuning (with the EvtGen package to describe the particle decays) instead of FONLL results in a central value of 40.4 (40.9) μb . A compilation of measurements of $d\sigma_{b\bar{b}}/dy$ at mid-rapidity is plotted in figure 7 as a function of \sqrt{s} , with superimposed FONLL predictions.

Finally, the total $b\bar{b}$ cross section was obtained as

$$\sigma(\text{pp} \rightarrow b\bar{b} + X) = \alpha_{4\pi} \frac{\sigma_{J/\psi \leftarrow h_B}(p_t^{J/\psi} > 1.3 \text{ GeV}/c, |y_{J/\psi}| < 0.9)}{2 \cdot BR(h_b \rightarrow J/\psi + X)}, \quad (4.3)$$

where $\alpha_{4\pi}$ is the ratio between the yield of J/ψ mesons (from the decay of b-hadrons) in the full phase space and the yield in the measured region $|y_{J/\psi}| < 0.9$ and $p_t^{J/\psi} > 1.3 \text{ GeV}/c$. The FONLL calculations provide $\alpha_{4\pi} = 4.49_{-0.10}^{+0.12}$, which produces $\sigma(\text{pp} \rightarrow b\bar{b} + X) = 282 \pm 74(\text{stat.})_{-68}^{+58}(\text{syst.})_{-7}^{+8}(\text{extr.}) \mu\text{b}$. The extrapolation factor $\alpha_{4\pi}$ was also estimated using PYTHIA with Perugia-0 tuning and found to be $\alpha_{4\pi}^{\text{PYTHIA}} = 4.20$. This measurement is in good agreement with those of the LHCb experiment, namely $288 \pm 4(\text{stat.}) \pm 48(\text{syst.}) \mu\text{b}$ and $284 \pm 20(\text{stat.}) \pm 49(\text{syst.}) \mu\text{b}$, which were based on the measured cross sections determined in the forward rapidity range from b-hadron decays into $J/\psi X$ and $D^0 \mu \nu X$, respectively [7, 24].

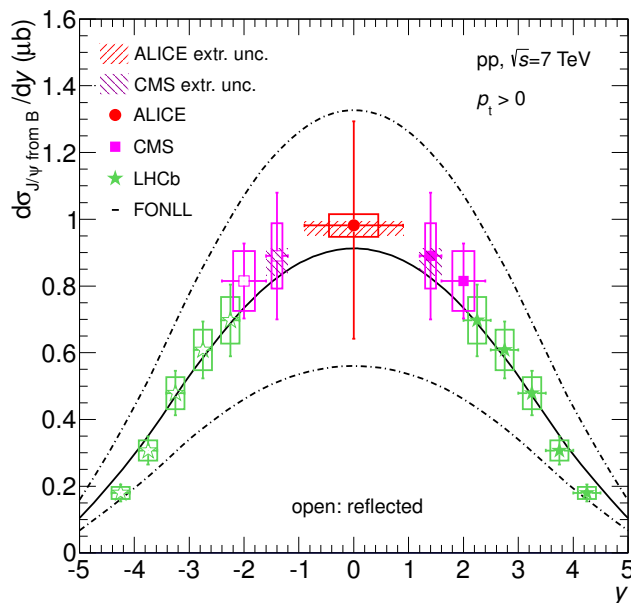


Figure 6. Cross section for non-prompt J/ψ production as a function of rapidity. The error bars represent the quadratic sum of the statistical and systematic errors, while the systematic uncertainties on luminosity and branching ratio are shown as boxes. The systematic uncertainties on the extrapolation to $p_t = 0$ are indicated by the slashed areas. The CMS values were obtained by integrating the published $d^2\sigma_{J/\psi \text{ from B}}/dp_t dy$ data measured for $1.2 < |y| < 1.6$ and $1.6 < |y| < 2.4$ [6]. The results obtained in the forward region by LHCb [7] are reflected with respect to $y = 0$ (open symbols). The FONLL calculation [41, 42] (and its uncertainty) is represented by solid (dashed) lines.

5 Summary

Results on the production cross section of prompt J/ψ and J/ψ from the decay of b-hadrons at mid-rapidity in pp collisions at $\sqrt{s} = 7$ TeV have been presented. The measured cross sections have been compared to theoretical predictions based on QCD and results from other experiments. Prompt J/ψ production is well described by NLO NRQCD models that include color-octet processes. The cross section of J/ψ from b-hadron decays is in good agreement with the FONLL prediction, based on perturbative QCD. The ALICE results at mid-rapidity, covering a lower p_t region down to $p_t = 1.3$ GeV/c, are complementary to those of the ATLAS and CMS experiments, which are available for J/ψ p_t above 6.5 GeV/c. Using the shape of the p_t and y distributions of b-quarks predicted by FONLL calculations, the mid-rapidity $d\sigma/dy$ and the total production cross section of $b\bar{b}$ pairs were determined.

Acknowledgments

The ALICE collaboration would like to thank all its engineers and technicians for their invaluable contributions to the construction of the experiment and the CERN accelerator

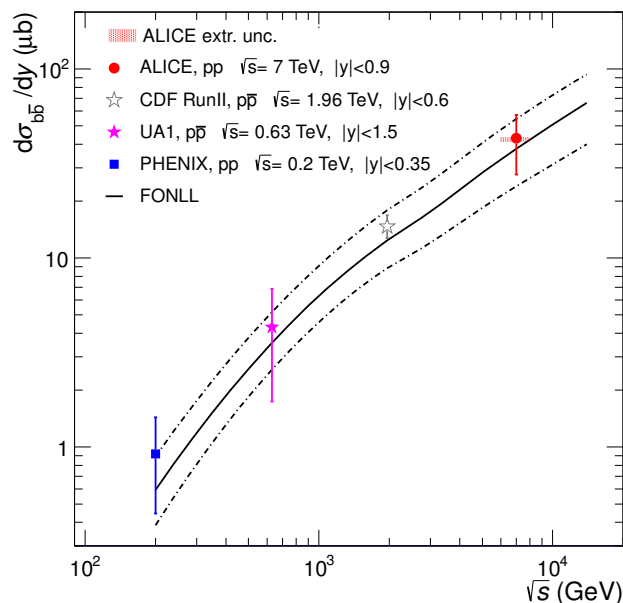


Figure 7. Beauty production cross section at mid-rapidity as a function of \sqrt{s} in pp (PHENIX [47] and ALICE results) and $p\bar{p}$ (UA1 [16] and CDF [17] results) collisions. The FONLL calculation [41, 42] (and its uncertainty) is represented by solid (dashed) lines.

teams for the outstanding performance of the LHC complex.

The ALICE collaboration would like to thank M. Butenschön and B.A. Kniehl, Y.-Q. Ma, K. Wang and K.T. Chao, and V.A. Saleev, M.A. Nefedov and A.V. Shipilova for providing their theoretical computations of the production cross section of prompt J/ψ , and M. Cacciari for predictions in the FONLL scheme.

The ALICE collaboration acknowledges the following funding agencies for their support in building and running the ALICE detector:

Calouste Gulbenkian Foundation from Lisbon and Swiss Fonds Kidagan, Armenia;

Conselho Nacional de Desenvolvimento Científico e Tecnológico (CNPq), Financiadora de Estudos e Projetos (FINEP), Fundação de Amparo à Pesquisa do Estado de São Paulo (FAPESP);

National Natural Science Foundation of China (NSFC), the Chinese Ministry of Education (CMOE) and the Ministry of Science and Technology of China (MSTC);

Ministry of Education and Youth of the Czech Republic;

Danish Natural Science Research Council, the Carlsberg Foundation and the Danish National Research Foundation;

The European Research Council under the European Community’s Seventh Framework Programme;

Helsinki Institute of Physics and the Academy of Finland;

French CNRS-IN2P3, the ‘Region Pays de Loire’, ‘Region Alsace’, ‘Region Auvergne’ and CEA, France;

German BMBF and the Helmholtz Association;
 General Secretariat for Research and Technology, Ministry of Development, Greece;
 Hungarian OTKA and National Office for Research and Technology (NKTH);
 Department of Atomic Energy and Department of Science and Technology of the Government of India;
 Istituto Nazionale di Fisica Nucleare (INFN) of Italy;
 MEXT Grant-in-Aid for Specially Promoted Research, Japan;
 Joint Institute for Nuclear Research, Dubna;
 National Research Foundation of Korea (NRF);
 CONACYT, DGAPA, México, ALFA-EC and the HELEN Program (High-Energy physics Latin-American–European Network);
 Stichting voor Fundamenteel Onderzoek der Materie (FOM) and the Nederlandse Organisatie voor Wetenschappelijk Onderzoek (NWO), Netherlands;
 Research Council of Norway (NFR);
 Polish Ministry of Science and Higher Education;
 National Authority for Scientific Research - NASR (Autoritatea Națională pentru Cercetare Științifică - ANCS);
 Federal Agency of Science of the Ministry of Education and Science of Russian Federation, International Science and Technology Center, Russian Academy of Sciences, Russian Federal Agency of Atomic Energy, Russian Federal Agency for Science and Innovations and CERN-INTAS;
 Ministry of Education of Slovakia;
 Department of Science and Technology, South Africa;
 CIEMAT, EELA, Ministerio de Educación y Ciencia of Spain, Xunta de Galicia (Consellería de Educación), CEADEN, Cubaenergía, Cuba, and IAEA (International Atomic Energy Agency);
 Swedish Research Council (VR) and Knut & Alice Wallenberg Foundation (KAW);
 Ukraine Ministry of Education and Science;
 United Kingdom Science and Technology Facilities Council (STFC);
 The United States Department of Energy, the United States National Science Foundation, the State of Texas, and the State of Ohio.

Open Access. This article is distributed under the terms of the Creative Commons Attribution License which permits any use, distribution and reproduction in any medium, provided the original author(s) and source are credited.

References

- [1] CDF collaboration, D. Acosta et al., *Measurement of the J/ψ meson and b -hadron production cross sections in $p\bar{p}$ collisions at $\sqrt{s} = 1960$ GeV*, *Phys. Rev. D* **71** (2005) 032001 [[hep-ex/0412071](#)] [[INSPIRE](#)].
- [2] CDF collaboration, A. Abulencia et al., *Polarization of J/ψ and ψ_{2S} mesons produced in $p\bar{p}$ collisions at $\sqrt{s} = 1.96$ TeV*, *Phys. Rev. Lett.* **99** (2007) 132001 [[arXiv:0704.0638](#)] [[INSPIRE](#)].

- [3] D0 collaboration, S. Abachi et al., *J/ψ production in p \bar{p} collisions at $\sqrt{s} = 1.8$ TeV*, *Phys. Lett. B* **370** (1996) 239 [INSPIRE].
- [4] D0 collaboration, B. Abbott et al., *Small angle J/ψ production in p \bar{p} collisions at $\sqrt{s} = 1.8$ TeV*, *Phys. Rev. Lett.* **82** (1999) 35 [hep-ex/9807029] [INSPIRE].
- [5] PHENIX collaboration, A. Adare et al., *J/ψ production versus transverse momentum and rapidity in p $^+$ p collisions at $\sqrt{s} = 200$ GeV*, *Phys. Rev. Lett.* **98** (2007) 232002 [hep-ex/0611020] [INSPIRE].
- [6] CMS collaboration, V. Khachatryan et al., *Prompt and non-prompt J/ψ production in pp collisions at $\sqrt{s} = 7$ TeV*, *Eur. Phys. J. C* **71** (2011) 1575 [arXiv:1011.4193] [INSPIRE].
- [7] LHCb collaboration, R. Aaij et al., *Measurement of J/ψ production in pp collisions at $\sqrt{s} = 7$ TeV*, *Eur. Phys. J. C* **71** (2011) 1645 [arXiv:1103.0423] [INSPIRE].
- [8] ATLAS collaboration, G. Aad et al., *Measurement of the differential cross-sections of inclusive, prompt and non-prompt J/ψ production in proton-proton collisions at $\sqrt{s} = 7$ TeV*, *Nucl. Phys. B* **850** (2011) 387 [arXiv:1104.3038] [INSPIRE].
- [9] ALICE collaboration, K. Aamodt et al., *Rapidity and transverse momentum dependence of inclusive J/ψ production in pp collisions at $\sqrt{s} = 7$ TeV*, *Phys. Lett. B* **704** (2011) 442 [Erratum: *ibid.* **B** (2012) in press] [arXiv:1105.0380] [INSPIRE].
- [10] CMS collaboration, S. Chatrchyan et al., *J/ψ and ψ_{2S} production in pp collisions at $\sqrt{s} = 7$ TeV*, *JHEP* **02** (2012) 011 [arXiv:1111.1557] [INSPIRE].
- [11] J. Lansberg, *On the mechanisms of heavy-quarkonium hadroproduction*, *Eur. Phys. J. C* **61** (2009) 693 [arXiv:0811.4005] [INSPIRE].
- [12] M. Butenschoen and B.A. Kniehl, *Reconciling J/ψ production at HERA, RHIC, Tevatron and LHC with NRQCD factorization at next-to-leading order*, *Phys. Rev. Lett.* **106** (2011) 022003 [arXiv:1009.5662] [INSPIRE].
- [13] Y.-Q. Ma, K. Wang and K.-T. Chao, *J/ψ (ψ′) production at the Tevatron and LHC at O(α_s⁴v⁴) in nonrelativistic QCD*, *Phys. Rev. Lett.* **106** (2011) 042002 [arXiv:1009.3655] [INSPIRE].
- [14] V. Saleev, M. Nefedov and A. Shipilova, *Prompt J/ψ production in the Regge limit of QCD: From Tevatron to LHC*, *Phys. Rev. D* **85** (2012) 074013 [arXiv:1201.3464] [INSPIRE].
- [15] UA1 collaboration, C. Albajar et al., *Measurement of the Bottom Quark Production Cross-Section in Proton - anti-Proton Collisions at $\sqrt{s} = 0.63$ TeV*, *Phys. Lett. B* **213** (1988) 405 [INSPIRE].
- [16] UA1 collaboration, C. Albajar et al., *Beauty production at the CERN p \bar{p} collider*, *Phys. Lett. B* **256** (1991) 121 [Erratum *ibid.* **B** **262** (1991) 497] [INSPIRE].
- [17] CDF collaboration, F. Abe et al., *Measurement of the B meson differential cross-section, dσ/dp_T, in p \bar{p} collisions at $\sqrt{s} = 1.8$ TeV*, *Phys. Rev. Lett.* **75** (1995) 1451 [hep-ex/9503013] [INSPIRE].
- [18] D0 collaboration, S. Abachi et al., *Inclusive μ and B quark production cross-sections in p \bar{p} collisions at $\sqrt{s} = 1.8$ TeV*, *Phys. Rev. Lett.* **74** (1995) 3548 [INSPIRE].
- [19] CDF collaboration, D. Acosta et al., *Measurement of the B⁺ total cross section and B⁺ differential cross section dσ/dp_T in p \bar{p} collisions at $\sqrt{s} = 1.8$ TeV*, *Phys. Rev. D* **65** (2002) 052005 [hep-ph/0111359] [INSPIRE].

- [20] HERA-B collaboration, Y. Zaitsev, *Investigation of heavy-quark production in proton-nucleus collisions with the HERA-B detector*, *Phys. Atom. Nucl.* **72** (2009) 675 [INSPIRE].
- [21] CMS collaboration, V. Khachatryan et al. *Measurement of the B^+ Production Cross Section in pp Collisions at $\sqrt{s} = 7$ TeV*, *Phys. Rev. Lett.* **106** (2011) 112001.
- [22] CMS collaboration, S. Chatrchyan et al., *Measurement of the B^0 production cross section in pp Collisions at $\sqrt{s} = 7$ TeV*, *Phys. Rev. Lett.* **106** (2011) 252001 [arXiv:1104.2892] [INSPIRE].
- [23] CMS collaboration, S. Chatrchyan et al., *Measurement of the Strange B Meson Production Cross Section with $J/\psi\phi$ Decays in pp Collisions at $\sqrt{s} = 7$ TeV*, *Phys. Rev. D* **84** (2011) 052008 [arXiv:1106.4048] [INSPIRE].
- [24] LHCb collaboration, R. Aaij et al., *Measurement of $\sigma(pp \rightarrow b\bar{b}X)$ at $\sqrt{s} = 7$ TeV in the forward region*, *Phys. Lett. B* **694** (2010) 209 [arXiv:1009.2731] [INSPIRE].
- [25] CMS collaboration, V. Khachatryan et al., *Inclusive b -hadron production cross section with muons in pp collisions at $\sqrt{s} = 7$ TeV*, *JHEP* **03** (2011) 090 [arXiv:1101.3512] [INSPIRE].
- [26] ALICE collaboration, K. Aamodt et al., *The ALICE experiment at the CERN LHC*, 2008 *JINST* **3** S08002 [INSPIRE].
- [27] ALICE collaboration, K. Aamodt et al., *Alignment of the ALICE Inner Tracking System with cosmic-ray tracks*, 2010 *JINST* **5** P03003 [arXiv:1001.0502] [INSPIRE].
- [28] J. Alme, Y. Andres, H. Appelshauer, S. Bablok, N. Bialas, et al., *The ALICE TPC, a large 3-dimensional tracking device with fast readout for ultra-high multiplicity events*, *Nucl. Instrum. Meth. A* **622** (2010) 316 [arXiv:1001.1950] [INSPIRE].
- [29] ALICE collaboration, B. Abelev et al., *Measurement of charm production at central rapidity in proton-proton collisions at $\sqrt{s} = 7$ TeV*, *JHEP* **01** (2012) 128 [arXiv:1111.1553] [INSPIRE].
- [30] PARTICLE DATA GROUP collaboration, K. Nakamura et al., *Review of particle physics*, *J. Phys. G* **37** (2010) 075021 [INSPIRE].
- [31] J.E. Gaiser, *Charmonium spectroscopy from radiative decays of the J/ψ and $J\psi'$* , Ph.D. Thesis, Stanford University, SLAC-R-255 (1982).
- [32] R. Brun et al., *CERN Program Library Long Write-up, W5013, GEANT Detector Description and Simulation Tool*, (1994).
- [33] D. Stocco et al., *Quarkonia detection with the ALICE Muon Spectrometer in pp collisions at $\sqrt{s} = 14$ TeV*, ALICE-INT-2006-029 <https://edms.cern.ch/document/803009/1>.
- [34] T. Sjöstrand, *High-energy physics event generation with PYTHIA 5.7 and JETSET 7.4*, *Comput. Phys. Commun.* **82** (1994) 74 [INSPIRE].
- [35] T. Sjöstrand, S. Mrenna and P.Z. Skands, *PYTHIA 6.4 Physics and Manual*, *JHEP* **05** (2006) 026 [hep-ph/0603175] [INSPIRE].
- [36] P.Z. Skands, *Tuning Monte Carlo Generators: The Perugia Tunes*, *Phys. Rev. D* **82** (2010) 074018 [arXiv:1005.3457] [INSPIRE].
- [37] D. Lange, *The EvtGen particle decay simulation package*, *Nucl. Instrum. Meth. A* **462** (2001) 152 [INSPIRE].

- [38] E. Barberio, B. van Eijk and Z. Was, *PHOTOS: A Universal Monte Carlo for QED radiative corrections in decays*, *Comput. Phys. Commun.* **66** (1991) 115 [[INSPIRE](#)].
- [39] E. Barberio and Z. Was, *PHOTOS: A Universal Monte Carlo for QED radiative corrections. Version 2.0*, *Comput. Phys. Commun.* **79** (1994) 291 [[INSPIRE](#)].
- [40] BABAR collaboration, B. Aubert et al., *Study of inclusive production of charmonium mesons in B decay*, *Phys. Rev. D* **67** (2003) 032002 [[hep-ex/0207097](#)] [[INSPIRE](#)].
- [41] M. Cacciari, S. Frixione, M. Mangano, P. Nason and G. Ridolfi, *QCD analysis of first b cross-section data at 1.96 TeV*, *JHEP* **07** (2004) 033 [[hep-ph/0312132](#)] [[INSPIRE](#)].
- [42] M. Cacciari, S. Frixione, N. Houdeau, M.L. Mangano, P. Nason, et al., *Theoretical predictions for charm and bottom production at the LHC*, *JHEP* **10** (2012) 137 [[arXiv:1205.6344](#)] [[INSPIRE](#)].
- [43] P.M. Nadolsky, H.-L. Lai, Q.-H. Cao, J. Huston, J. Pumplin, et al., *Implications of CTEQ global analysis for collider observables*, *Phys. Rev. D* **78** (2008) 013004 [[arXiv:0802.0007](#)] [[INSPIRE](#)].
- [44] DELPHI collaboration, P. Abreu et al., *J/ψ production in the hadronic decays of the Z*, *Phys. Lett. B* **341** (1994) 109 [[INSPIRE](#)].
- [45] L3 collaboration, O. Adriani et al., *χ_c production in hadronic Z decays*, *Phys. Lett. B* **317** (1993) 467 [[INSPIRE](#)].
- [46] ALEPH collaboration, D. Buskulic et al., *Measurements of mean lifetime and branching fractions of b hadrons decaying to J/ψ*, *Phys. Lett. B* **295** (1992) 396 [[INSPIRE](#)].
- [47] PHENIX collaboration, A. Adare et al., *Measurement of Bottom versus Charm as a Function of Transverse Momentum with Electron-Hadron Correlations in p⁺p Collisions at √s = 200 GeV*, *Phys. Rev. Lett.* **103** (2009) 082002 [[arXiv:0903.4851](#)] [[INSPIRE](#)].

The ALICE collaboration

Betty Abelev,^{cp} Jaroslav Adam,^{bg} Dagmar Adamova,^{cu} Andrew Marshall Adare,^{ep} Madan Aggarwal,^{cy} Gianluca Aglieri Rinella,^{bc} Andras Gabor Agocs,^{ch} Andrea Agostinelli,^{au} Saul Aguilar Salazar,^{cd} Zubayer Ahammed,^{el} Arshad Ahmad,^{am} Nazeer Ahmad,^{am} Sul-Ah Ahn,^{cj} Sang Un Ahn,^{ck,bj} Alexander Akindinov,^{bt} Dmitry Aleksandrov,^{dj} Bruno Alessandro,^{dp} Jose Ruben Alfaro Molina,^{cd} Andrea Alici,^{ds,ai} Anton Alkin,^{ab} Erick Jonathan Almaraz Avina,^{cd} Johan Alme,^{be} Torsten Alt,^{bi} Valerio Altini,^{ba} Sedat Altinpinar,^{an} Igor Altsybeev,^{em} Cristian Andrei,^{cr} Anton Andronic,^{dg} Venelin Anguelov,^{dd} Jonas Anielski,^{cb} Christopher Daniel Anson,^{ao} Tome Anticic,^{dh} Federico Antinori,^{do} Pietro Antonioli,^{ds} Laurent Bernard Aphetche,^{dx} Harald Appelshauser,^{bz} Nicolas Arbor,^{cl} Silvia Arcelli,^{au} Andreas Arend,^{bz} Nestor Armesto,^{al} Roberta Araldi,^{dp} Tomas Robert Aronsson,^{ep} Ionut Cristian Arsene,^{dg} Mesut Arslandok,^{bz} Andzhey Asryan,^{em} Andre Augustinus,^{bc} Ralf Peter Averbeck,^{dg} Terry Awes,^{cv} Juha Heikki Aysto,^{bk} Mohd Danish Azmi,^{am} Matthias Jakob Bach,^{bi} Angela Badala,^{du} Yong Wook Baek,^{ck,bj} Raphaelle Marie Bailhache,^{bz} Renu Bala,^{dp} Rinaldo Baldini Ferroli,^{ai} Alberto Baldisseri,^{ak} Alain Baldit,^{ck} Fernando Baltasar Dos Santos Pedrosa,^{bc} Jaroslav Ban,^{bu} Rama Chandra Baral,^{bv} Roberto Barbera,^{aw} Francesco Barile,^{ba} Gergely Gabor Barnafoldi,^{ch} Lee Stuart Barnby,^{dl} Valerie Barret,^{ck} Jerzy Gustaw Bartke,^{dz} Maurizio Basile,^{au} Nicole Bastid,^{ck} Sumit Basu,^{el} Bastian Bathen,^{cb} Guillaume Batigne,^{dx} Boris Batyunya,^{cg} Christoph Heinrich Baumann,^{bz} Ian Gardner Bearden,^{cs} Hans Beck,^{bz} Nirbhay Kumar Behera,^{bn} Iouri Belikov,^{cf} Francesca Bellini,^{au} Rene Bellwied,^{ef} Ernesto Belmont-Moreno,^{cd} Gyula Bencedi,^{ch} Stefania Beole,^{ay} Ionela Berceanu,^{cr} Alexandru Bercuci,^{cr} Yaroslav Berdnikov,^{cw} Daniel Berenyi,^{ch} Anais Annick Erica Bergognon,^{dx} Dario Berzano,^{dp} Latchezar Betev,^{bc} Anju Bhasin,^{db} Ashok Kumar Bhati,^{cy} Jihyun Bhom,^{ej} Livio Bianchi,^{ay} Nicola Bianchi,^{cm} Chiara Bianchin,^{as} Jaroslav Bielcik,^{bg} Jana Bielcikova,^{cu} Ante Bilandzic,^{ct,cs} Sandro Bjelogrić,^{bs} F. Blanco,^{ag} Francesco Blanco,^{ef} Dmitry Blau,^{dj} Christoph Blume,^{bz} Marco Boccioni,^{bc} Nicolas Bock,^{ao} Stefan Boettger,^{by} Alexey Bogdanov,^{cq} Hans Boggild,^{cs} Mikhail Bogolyubsky,^{bq} Laszlo Boldizsar,^{ch} Marek Bombara,^{bh} Julian Book,^{bz} Herve Borel,^{ak} Alexander Borissov,^{eo} Suwendu Nath Bose,^{dk} Francesco Bossu,^{ay} Michiel Botje,^{ct} Bruno Alexandre Boyer,^{bp} Ermes Braidot,^{co} Peter Braun-Munzinger,^{dg} Marco Bregant,^{dx} Timo Gunther Breitner,^{by} Tyler Allen Browning,^{de} Michal Broz,^{bf} Rene Brun,^{bc} Elena Bruna,^{ay,dp} Giuseppe Eugenio Bruno,^{ba} Dmitry Budnikov,^{di} Henner Buesching,^{bz} Stefania Bufalino,^{ay,dp} Kyrylo Bugaiev,^{ab} Oliver Busch,^{dd} Edith Zinhle Buthelezi,^{da} Diego Caballero Orduna,^{ep} Davide Caffarri,^{as} Xu Cai,^{bm} Helen Louise Caines,^{ep} Ernesto Calvo Villar,^{dm} Paolo Camerini,^{at} Veronica Canoa Roman,^{ah,aa} Giovanni Cara Romeo,^{ds} Francesco Carena,^{bc} Wisla Carena,^{bc} Nelson Carlin Filho,^{ec} Federico Carminati,^{bc} Camilo Andres Carrillo Montoya,^{bc} Amaya Ofelia Casanova Diaz,^{cm} Javier Ernesto Castillo Castellanos,^{ak} Juan Francisco Castillo Hernandez,^{dg} Ester Anna Rita Casula,^{ar} Vasile Catanescu,^{cr} Costanza Cavicchioli,^{bc} Cesar Ceballos Sanchez,^{af} Jan Cepila,^{bg} Piergiorgio Cerello,^{dp} Beomsu Chang,^{bk,es} Sylvain Chapeland,^{bc} Jean-Luc Fernand Charvet,^{ak} Subhasis Chattopadhyay,^{el} Sukalyan Chattopadhyay,^{dk} Isha Chawla,^{cy} Michael Gerard Cherney,^{cx} Cvetan Cheshkov,^{bc,ee} Brigitte Cheynis,^{ee} Vasco

Miguel Chibante Barroso,^{bc} David Chinellato,^{ed} Peter Chochula,^{bc} Marek Chojnacki,^{bs}
 Subikash Choudhury,^{el} Panagiotis Christakoglou,^{ct,bs} Christian Holm Christensen,^{cs} Peter
 Christiansen,^{bb} Tatsuya Chujo,^{ej} Suh-Urk Chung,^{df} Corrado Cicalo,^{dr} Luisa
 Cifarelli,^{au,bc,ai} Federico Cindolo,^{ds} Jean Willy Andre Cleymans,^{da} Fabrizio Coccetti,^{ai}
 Fabio Colamaria,^{ba} Domenico Colella,^{ba} Gustavo Conesa Balbastre,^{cl} Zaida Conesa del
 Valle,^{bc} Paul Constantin,^{dd} Giacomo Contin,^{at} Jesus Guillermo Contreras,^{ah} Thomas
 Michael Cormier,^{eo} Yasser Corrales Morales,^{ay} Pietro Cortese,^{az} Ismael Cortes
 Maldonado,^{aa} Mauro Rogerio Cosentino,^{co} Filippo Costa,^{bc} Manuel Enrique Cotallo,^{ag}
 Elisabetta Crescio,^{ah} Philippe Crochet,^{ck} Emilia Cruz Alaniz,^{cd} Eleazar Cuautle,^{cc} Leticia
 Cunqueiro,^{cm} Andrea Dainese,^{as,do} Hans Hjersing Dalsgaard,^{cs} Andrea Danu,^{bx} Debasish
 Das,^{dk} Indranil Das,^{bp} Kushal Das,^{dk} Sadhana Dash,^{bn} Ajay Kumar Dash,^{ed} Sudipan
 De,^{el} Gabriel de Barros,^{ec} Annalisa De Caro,^{ax,ai} Giacinto de Cataldo,^{dt} Jan de
 Cuveland,^{bi} Alessandro De Falco,^{ar} Daniele De Gruttola,^{ax} Hugues Delagrangue,^{dx}
 Andrzej Deloff,^{dv} Vyacheslav Demanov,^{di} Nora De Marco,^{dp} Ervin Denes,^{ch} Salvatore De
 Pasquale,^{ax} Airton Deppman,^{ec} Ginevra D'Erasmus,^{ba} Raoul Stefan de Rooij,^{bs} Miguel
 Angel Diaz Corchero,^{ag} Domenico Di Bari,^{ba} Carmelo Di Giglio,^{ba} Thomas Dietel,^{cb}
 Sergio Di Liberto,^{dq} Antonio Di Mauro,^{bc} Pasquale Di Nezza,^{cm} Roberto Divia,^{bc}
 Oeystein Djuvslund,^{an} Alexandru Florin Dobrin,^{eo,bb} Tadeusz Antoni Dobrowolski,^{dv}
 Isabel Dominguez,^{cc} Benjamin Donigus,^{dg} Olja Dordic,^{aq} Olga Driga,^{dx} Anand Kumar
 Dubey,^{el} Laurent Ducroux,^{ee} Pascal Dupieux,^{ck} Mihir Ranjan Dutta Majumdar,^{el} A.K.
 Dutta Majumdar,^{dk} Domenico Elia,^{dt} David Philip Emschermann,^{cb} Heiko Engel,^{by} Hege
 Austrheim Erdal,^{be} Bruno Espagnon,^{bp} Magali Danielle Estienne,^{dx} Shinichi Esumi,^{ej}
 David Evans,^{dl} Gyulnara Eyyubova,^{aq} Daniela Fabris,^{as,do} Julien Faivre,^{cl} Davide
 Falchieri,^{au} Alessandra Fantoni,^{cm} Markus Fasel,^{dg} Roger Worsley Fearick,^{da} Anatoly
 Fedunov,^{cg} Dominik Fehlker,^{an} Linus Feldkamp,^{cb} Daniel Felea,^{bx} Bo Fenton-Olsen,^{co}
 Grigory Feofilov,^{em} Arturo Fernandez Tellez,^{aa} Alessandro Ferretti,^{ay} Roberta Ferretti,^{az}
 Jan Figiel,^{dz} Marcel Figueredo,^{ec} Sergey Filchagin,^{di} Dmitry Finogeev,^{br} Fiorella
 Fionda,^{ba} Enrichetta Maria Fiore,^{ba} Michele Floris,^{bc} Siegfried Valentin Foertsch,^{da}
 Panagiota Foka,^{dg} Sergey Fokin,^{dj} Enrico Fragiacommo,^{dn} Ulrich Michael Frankenfeld,^{dg}
 Ulrich Fuchs,^{bc} Christophe Furget,^{cl} Mario Fusco Girard,^{ax} Jens Joergen Gaardhoje,^{cs}
 Martino Gagliardi,^{ay} Alberto Gago,^{dm} Mauro Gallio,^{ay} Dhevan Raja Gangadharan,^{ao}
 Paraskevi Ganoti,^{cv} Jose Garabatos,^{dg} Edmundo Garcia-Solis,^{aj} Irakli Garishvili,^{cp}
 Jochen Gerhard,^{bi} Marie Germain,^{dx} Claudio Geuna,^{ak} Andrei George Gheata,^{bc} Mihaela
 Gheata,^{bx,bc} Bruno Ghidini,^{ba} Premomoy Ghosh,^{el} Paola Gianotti,^{cm} Martin Robert
 Girard,^{en} Paolo Giubellino,^{bc} Ewa Gladysz-Dziadus,^{dz} Peter Glassel,^{dd} Ramon Gomez,^{eb}
 Alexey Gonschior,^{dg} Elena Gonzalez Ferreira,^{al} Laura Helena Gonzalez-Trueba,^{cd} Pedro
 Gonzalez-Zamora,^{ag} Sergey Gorbunov,^{bi} Ankita Goswami,^{dc} Sven Gotovac,^{dy} Varlen
 Grabski,^{cd} Lukasz Kamil Graczykowski,^{en} Robert Grajcarek,^{dd} Alessandro Grelli,^{bs}
 Costin Grigoras,^{bc} Alina Gabriela Grigoras,^{bc} Vladislav Grigoriev,^{cq} Ara Grigoryan,^{eq}
 Smbat Grigoryan,^{cg} Boris Grinyov,^{ab} Nevio Grion,^{dn} Philippe Gros,^{bb} Jan Fiete
 Grosse-Oetringhaus,^{bc} Jean-Yves Grossiord,^{ee} Raffaele Grosso,^{bc} Fedor Guber,^{br} Rachid
 Guernane,^{cl} Cesar Guerra Gutierrez,^{dm} Barbara Guerzoni,^{au} Maxime Rene Joseph
 Guilbaud,^{ee} Kristjan Herlache Gulbrandsen,^{cs} Taku Gunji,^{ei} Anik Gupta,^{db} Ramni

Gupta,^{db} Hans Gutbrod,^{dg} Oystein Senneset Haaland,^{an} Cynthia Marie Hadjidakis,^{bp} Maria Haiduc,^{bx} Hideki Hamagaki,^{ei} Gergoe Hamar,^{ch} Byounghee Han,^{ap} Luke David Hanratty,^{dl} Alexander Hansen,^{cs} Zuzana Harmanova,^{bh} John William Harris,^{ep} Matthias Hartig,^{bz} Dumitru Hasegan,^{bx} Despoina Hatzifotiadou,^{ds} Arsen Hayrapetyan,^{bc,eq} Stefan Thomas Heckel,^{bz} Markus Ansgar Heide,^{cb} Haavard Helstrup,^{be} Andrei Ionut Herghelegiu,^{cr} Gerardo Antonio Herrera Corral,^{ah} Norbert Herrmann,^{dd} Benjamin Andreas Hess,^{ek} Kristin Fanebust Hetland,^{be} Bernard Hicks,^{ep} Per Thomas Hille,^{ep} Boris Hippolyte,^{cf} Takuma Horaguchi,^{ej} Yasuto Hori,^{ei} Peter Zahariev Hristov,^{bc} Ivana Hrivnacova,^{bp} Meidana Huang,^{an} Thomas Humanic,^{ao} Dae Sung Hwang,^{ap} Raphaelle Ichou,^{ck} Radiy Ilkaev,^{di} Iryna Ilkiv,^{dv} Motoi Inaba,^{ej} Elisa Incani,^{ar} Gian Michele Innocenti,^{ay} Pier Giorgio Innocenti,^{bc} Mikhail Ippolitov,^{dj} Muhammad Irfan,^{am} Cristian George Ivan,^{dg} Vladimir Ivanov,^{cw} Marian Ivanov,^{dg} Andrey Ivanov,^{em} Oleksii Ivanytskyi,^{ab} Adam Wlodzimierz Jacholkowski,^{bc} Peter Jacobs,^{co} Haeng Jin Jang,^{cj} Swensy Gwladys Jangal,^{cf} Malgorzata Anna Janik,^{en} Rudolf Janik,^{bf} Sandun Jayarathna,^{ef} Satyajit Jena,^{bn} Deeptanshu Manu Jha,^{eo} Raul Tonatiuh Jimenez Bustamante,^{cc} Lennart Jirden,^{bc} Peter Graham Jones,^{dl} Hyung Taik Jung,^{bj} Anton Jusko,^{dl} Alexei Kaidalov,^{bt} Vanik Kakoyan,^{eq} Sebastian Kalcher,^{bi} Peter Kalinak,^{bu} Tuomo Esa Aukusti Kalliokoski,^{bk} Alexander Philipp Kalweit,^{ca} Kalliopi Kanaki,^{an} Ju Hwan Kang,^{es} Vladimir Kaplin,^{cq} Ayben Karasu Uysal,^{bc,er} Oleg Karavichev,^{br} Tatiana Karavicheva,^{br} Evgeny Karpechev,^{br} Andrey Kazantsev,^{dj} Udo Wolfgang Kebschull,^{by} Ralf Keidel,^{et} Palash Khan,^{dk} Mohisin Mohammed Khan,^{am} Shuaib Ahmad Khan,^{el} Alexei Khanzadeev,^{cw} Yury Kharlov,^{bq} Bjarte Kileng,^{be} Do Won Kim,^{bj} Mimae Kim,^{bj} Minwoo Kim,^{es} Seon Hee Kim,^{bj} Dong Jo Kim,^{bk} Se Yong Kim,^{ap} Jonghyun Kim,^{ap} Jin Sook Kim,^{bj} Beomkyu Kim,^{es} Taesoo Kim,^{es} Stefan Kirsch,^{bi} Ivan Kisel,^{bi} Sergey Kiselev,^{bt} Adam Ryszard Kisiel,^{bc,en} Jennifer Lynn Klay,^{ad} Jochen Klein,^{dd} Christian Klein-Bosing,^{cb} Michael Kliemant,^{bz} Alexander Kluge,^{bc} Michael Linus Knichel,^{dg} Anders Garritt Knospe,^{ea} Kathrin Koch,^{dd} Markus Kohler,^{dg} Anatoly Kolojvari,^{em} Valery Kondratiev,^{em} Natalia Kondratyeva,^{cq} Artem Konevskih,^{br} Andrey Korneev,^{di} Ravjeet Kour,^{dl} Marek Kowalski,^{dz} Serge Kox,^{cl} Greeshma Koyithatta Meethalevedu,^{bn} Jiri Kral,^{bk} Ivan Kralik,^{bu} Frederick Kramer,^{bz} Ingrid Christine Kraus,^{dg} Tobias Krawutschke,^{dd,bd} Michal Krelina,^{bg} Matthias Kretz,^{bi} Marian Krivda,^{dl,bu} Filip Krizek,^{bk} Miroslav Krus,^{bg} Evgeny Kryshen,^{cw} Mikolaj Krzewicki,^{dg} Yury Kucheriaev,^{dj} Christian Claude Kuhn,^{cf} Paul Kuijjer,^{ct} Igor Kulakov,^{bz} Jitendra Kumar,^{bn} Podist Kurashvili,^{dv} A.B. Kurepin,^{br} A. Kurepin,^{br} Alexey Kuryakin,^{di} Vasily Kushpil,^{cu} Svetlana Kushpil,^{cu} Henning Kvaerno,^{aq} Min Jung Kweon,^{dd} Youngil Kwon,^{es} Pedro Ladron de Guevara,^{cc} Igor Lakomov,^{bp} Rune Langoy,^{an} Sarah Louise La Pointe,^{bs} Camilo Ernesto Lara,^{by} Antoine Xavier Lardeux,^{dx} Paola La Rocca,^{aw} Cristina Lazzeroni,^{dl} Ramona Lea,^{at} Yves Le Bornec,^{bp} Mateusz Lechman,^{bc} Sung Chul Lee,^{bj} Ki Sang Lee,^{bj} Graham Richard Lee,^{dl} Frederic Lefevre,^{dx} Joerg Walter Lehnert,^{bz} Lars Leistam,^{bc} Matthieu Laurent Lenhardt,^{dx} Vito Lenti,^{dt} Hermes Leon,^{cd} Marco Leoncino,^{dp} Ildefonso Leon Monzon,^{eb} Hermes Leon Vargas,^{bz} Peter Levai,^{ch} Jorgen Lien,^{an} Roman Lietava,^{dl} Svein Lindal,^{aq} Volker Lindenstruth,^{bi} Christian Lippmann,^{dg,bc} Michael Annan Lisa,^{ao} Lijiao Liu,^{an} Per-Ivar Loenne,^{an} Vera Loggins,^{eo} Vitaly Loginov,^{cq} Stefan Bernhard Lohn,^{bc} Daniel

Lohner,^{dd} Constantinos Loizides,^{co} Kai Krister Loo,^{bk} Xavier Bernard Lopez,^{ck} Ernesto Lopez Torres,^{af} Gunnar Lovhoiden,^{aq} Xianguo Lu,^{dd} Philipp Luettig,^{bz} Marcello Lunardon,^{as} Jiebin Luo,^{bm} Grazia Luparello,^{bs} Lionel Luquin,^{dx} Cinzia Luzzi,^{bc} Rongrong Ma,^{ep} Ke Ma,^{bm} Dilan Minthaka Madagadahettige-Don,^{ef} Alla Maevskaya,^{br} Magnus Mager,^{ca,bc} Durga Prasad Mahapatra,^{bv} Antonin Maire,^{dd} Mikhail Malaev,^{cw} Ivonne Alicia Maldonado Cervantes,^{cc} Ludmila Malinina,^{cg,1} Dmitry Mal'Kevich,^{bt} Peter Malzacher,^{dg} Alexander Mamonov,^{di} Loic Henri Antoine Manceau,^{dp} Lalit Kumar Mangotra,^{db} Vladislav Manko,^{dj} Franck Manso,^{ck} Vito Manzari,^{dt} Yaxian Mao,^{bm} Massimiliano Marchisone,^{ck,ay} Jiri Mares,^{bv} Giacomo Vito Margagliotti,^{at,dn} Anselmo Margotti,^{ds} Ana Maria Marin,^{dg} Cesar Augusto Marin Tobon,^{bc} Christina Markert,^{ea} Irakli Martashvili,^{eh} Paolo Martinengo,^{bc} Mario Ivan Martinez,^{aa} Arnulfo Martinez Davalos,^{cd} Gines Martinez Garcia,^{dx} Yevgen Martynov,^{ab} Alexis Jean-Michel Mas,^{dx} Silvia Masciocchi,^{dg} Massimo Maserà,^{ay} Alberto Masoni,^{dr} Laure Marie Massacrier,^{ee,dx} Mario Mastromarco,^{dt} Annalisa Mastroserio,^{ba,bc} Zoe Louise Matthews,^{dl} Adam Tomasz Matyja,^{dz,dx} Daniel Mayani,^{cc} Christoph Mayer,^{dz} Joel Mazer,^{eh} Alessandra Maria Mazzoni,^{dq} Franco Meddi,^{av} Arturo Alejandro Menchaca-Rocha,^{cd} Jorge Mercado Perez,^{dd} Michal Meres,^{bf} Yasuo Miake,^{ej} Leonardo Milano,^{ay} Jovan Milosevic,^{aq,2} Andre Mischke,^{bs} Aditya Nath Mishra,^{dc} Dariusz Miskowicz,^{dg,bc} Ciprian Mihai Mitu,^{bx} Jocelyn Mlynarz,^{eo} Bedangadas Mohanty,^{el} Ajit Kumar Mohanty,^{bc} Levente Molnar,^{bc} Luis Manuel Montano Zetina,^{ah} Marco Monteno,^{dp} Esther Montes,^{ag} Taebong Moon,^{es} Maurizio Morando,^{as} Denise Aparecida Moreira De Godoy,^{ec} Sandra Moretto,^{as} Andreas Morsch,^{bc} Valeria Muccifora,^{cm} Eugen Mudnic,^{dy} Sanjib Muhuri,^{el} Maitreyee Mukherjee,^{el} Hans Muller,^{bc} Marcelo Munhoz,^{ec} Luciano Musa,^{bc} Alfredo Musso,^{dp} Basanta Kumar Nandi,^{bn} Rosario Nania,^{ds} Eugenio Nappi,^{dt} Christine Nattrass,^{eh} Nikolay Naumov,^{di} Sparsh Navin,^{dl} Tapan Kumar Nayak,^{el} Sergey Nazarenko,^{di} Gleb Nazarov,^{di} Alexander Nedosekin,^{bt} Maria Nicassio,^{ba} Mihai Niculescu,^{bx,bc} Borge Svane Nielsen,^{cs} Takafumi Niida,^{ej} Sergey Nikolaev,^{dj} Vedran Nikolic,^{dh} Sergey Nikulin,^{dj} Vladimir Nikulin,^{cw} Bjorn Steven Nilsen,^{cx} Mads Stormo Nilsson,^{aq} Francesco Noferini,^{ds,ai} Petr Nomokonov,^{cg} Gerardus Nooren,^{bs} Norbert Novitzky,^{bk} Alexandre Nyanin,^{dj} Anitha Nyatha,^{bn} Casper Nygaard,^{cs} Joakim Ingemar Nystrand,^{an} Alexander Ochirov,^{em} Helmut Oskar Oeschler,^{ca,bc} Saehanseul Oh,^{ep} Sun Kun Oh,^{bj} Janusz Oleniacz,^{en} Chiara Oppedisano,^{dp} Antonio Ortiz Velasquez,^{bb,cc} Giacomo Ortona,^{ay} Anders Nils Erik Oskarsson,^{bb} Piotr Krystian Ostrowski,^{en} Jacek Tomasz Otwinowski,^{dg} Ken Oyama,^{dd} Kyoichiro Ozawa,^{ei} Yvonne Chiara Pachmayer,^{dd} Milos Pachr,^{bg} Fatima Padilla,^{ay} Paola Pagano,^{ax} Guy Paic,^{cc} Florian Painke,^{bi} Carlos Pajares,^{al} S. Pal,^{ak} Susanta Kumar Pal,^{el} Arvinder Singh Palaha,^{dl} Armando Palmeri,^{du} Vardanush Papikyan,^{eq} Giuseppe Pappalardo,^{du} Woo Jin Park,^{dg} Annika Passfeld,^{cb} Blahoslav Pastircak,^{bu} Dmitri Ivanovich Patalakha,^{bq} Vincenzo Patocchio,^{dt} Alexei Pavlinov,^{eo} Tomasz Jan Pawlak,^{en} Thomas Peitzmann,^{bs} Hugo Denis Antonio Pereira Da Costa,^{ak} Elienos Pereira De Oliveira Filho,^{ec} Dmitri Peresunko,^{dj}

³Also at M.V.Lomonosov Moscow State University, D.V.Skobel'tsyn Institute of Nuclear Physics, Moscow, Russia.

⁴Also at University of Belgrade, Faculty of Physics and "Vinča" Institute of Nuclear Sciences, Belgrade, Serbia.

Carlos Eugenio Perez Lara,^{ct} Edgar Perez Lezama,^{cc} Diego Perini,^{bc} Davide Perrino,^{ba}
 Wiktor Stanislaw Peryt,^{en} Alessandro Pesci,^{ds} Vladimir Peskov,^{bc,cc} Yury Pestov,^{ac}
 Vojtech Petracek,^{bg} Michal Petran,^{bg} Mariana Petris,^{cr} Plamen Rumenov Petrov,^{dl} Mihai
 Petrovici,^{cr} Catia Petta,^{aw} Stefano Piano,^{dn} Anna Piccotti,^{dp} Miroslav Pikna,^{bf} Philippe
 Pillot,^{dx} Ombretta Pinazza,^{bc} Lawrence Pinsky,^{ef} Nora Pitz,^{bz} Danthasinghe
 Piyarathna,^{ef} Mateusz Andrzej Ploskon,^{co} Jan Marian Pluta,^{en} Timur Pocheptsov,^{cg}
 Sona Pochybova,^{ch} Pedro Luis Manuel Podesta Lerma,^{eb} Martin Poghosyan,^{bc,ay} Karel
 Polak,^{bw} Boris Polichtchouk,^{bq} Amalia Pop,^{cr} Sarah Porteboeuf-Houssais,^{ck} Vladimir
 Pospisil,^{bg} Baba Potukuchi,^{db} Sidharth Kumar Prasad,^{eo} Roberto Preghenella,^{ds,ai}
 Francesco Prino,^{dp} Claude Andre Pruneau,^{eo} Igor Pshenichnov,^{br} Sergey Puchagin,^{di}
 Giovanna Puddu,^{ar} Jordi Pujol Teixido,^{by} Alberto Pulvirenti,^{aw,bc} Valery Punin,^{di} Marian
 Putis,^{bh} Jorn Henning Putschke,^{eo,ep} Emanuele Quercigh,^{bc} Henrik Qvigstad,^{aq} Alexandre
 Rachevski,^{dn} Alphonse Rademakers,^{bc} Sylwester Radomski,^{dd} Tomi Samuli Raiha,^{bk} Jan
 Rak,^{bk} Andry Malala Rakotozafindrabe,^{ak} Luciano Ramello,^{az} Abdiel Ramirez Reyes,^{ah}
 Sudhir Raniwala,^{dc} Rashmi Raniwala,^{dc} Sami Sakari Rasanen,^{bk} Bogdan Theodor
 Rascanu,^{bz} Deepika Rathee,^{cy} Kenneth Francis Read,^{eh} Jean-Sebastien Real,^{cl} Krzysztof
 Redlich,^{dv,ce} Patrick Reichelt,^{bz} Martijn Reicher,^{bs} Rainer Arno Ernst Renfordt,^{bz} Anna
 Rita Reolon,^{cm} Andrey Reshetin,^{br} Felix Vincenz Rettig,^{bi} Jean-Pierre Revol,^{bc} Klaus
 Johannes Reygers,^{dd} Lodovico Riccati,^{dp} Renato Angelo Ricci,^{cn} Tuva Richert,^{bb} Matthias
 Rudolph Richter,^{aq} Petra Riedler,^{bc} Werner Riegler,^{bc} Francesco Riggi,^{aw,du} Bartolomeu
 Rodrigues Fernandes Rabacal,^{bc} Mario Rodriguez Cahuantzi,^{aa} Alis Rodriguez Manso,^{ct}
 Ketil Roed,^{an} David Rohr,^{bi} Dieter Rohrich,^{an} Rosa Romita,^{dg} Federico Ronchetti,^{cm}
 Philippe Rosnet,^{ck} Stefan Rossegger,^{bc} Andrea Rossi,^{bc,as} Christelle Sophie Roy,^{cf} Pradip
 Kumar Roy,^{dk} Antonio Juan Rubio Montero,^{ag} Rinaldo Rui,^{at} Evgeny Ryabinkin,^{dj}
 Andrzej Rybicki,^{dz} Sergey Sadovsky,^{bq} Karel Safarik,^{bc} Raghunath Sahoo,^{bo} Pradip
 Kumar Sahu,^{bv} Jogender Saini,^{el} Hiroaki Sakaguchi,^{bl} Shingo Sakai,^{co} Dosatsu Sakata,^{ej}
 Carlos Albert Salgado,^{al} Jai Salzwedel,^{ao} Sanjeev Singh Sambyal,^{db} Vladimir
 Samsonov,^{cw} Xitzel Sanchez Castro,^{cf} Ladislav Sandor,^{bu} Andres Sandoval,^{cd} Satoshi
 Sano,^{ei} Masato Sano,^{ej} Rainer Santo,^{cb} Romualdo Santoro,^{dt,bc,ai} Juho Jaako Sarkamo,^{bk}
 Eugenio Scapparone,^{ds} Fernando Scarlassara,^{as} Rolf Paul Scharenberg,^{de} Claudiu Cornel
 Schiaua,^{cr} Rainer Martin Schicker,^{dd} Christian Joachim Schmidt,^{dg} Hans Rudolf
 Schmidt,^{ek} Steffen Schreiner,^{bc} Simone Schuchmann,^{bz} Jurgen Schukraft,^{bc} Yves Roland
 Schutz,^{bc,dx} Kilian Eberhard Schwarz,^{dg} Kai Oliver Schweda,^{dg,dd} Gilda Scioli,^{au} Enrico
 Scomparin,^{dp} Rebecca Scott,^{eh} Patrick Aaron Scott,^{dl} Gianfranco Segato,^{as} Ilya
 Selioujenkov,^{dg} Serhiy Senyukov,^{az,cf} Jeewon Seo,^{df} Sergio Serci,^{ar} Eulogio Serradilla,^{ag,cd}
 Adrian Sevcenco,^{bx} Alexandre Shabetai,^{dx} Galina Shabratova,^{cg} Ruben Shahoyan,^{bc}
 Natasha Sharma,^{cy} Satish Sharma,^{db} Rohini Sharma,^{db} Kenta Shigaki,^{bl} Maya
 Shimomura,^{ej} Katherin Shtejer,^{af} Yury Sibiriak,^{dj} Melinda Siciliano,^{ay} Eva Sicking,^{bc}
 Sabyasachi Siddhanta,^{dr} Teodor Siemiarczuk,^{dv} David Olle Rickard Silvermyr,^{cv}
 Catherine Silvestre,^{cl} Goran Simatovic,^{cc,dh} Giuseppe Simonetti,^{bc} Rama Narayana
 Singaraju,^{el} Ranbir Singh,^{db} Subhash Singha,^{el} Vikas Singhal,^{el} Tinku Sinha,^{dk} Bikash
 Sinha,^{el} Branislav Sitar,^{bf} Mario Sitta,^{az} Bernhard Skaali,^{aq} Kyrre Skjerdal,^{an} Radek
 Smakal,^{bg} Nikolai Smirnov,^{ep} Raimond Snellings,^{bs} Carsten Sogaard,^{cs} Ron Ariel Soltz,^{cp}

Hyungsuk Son,^{ap} Myunggeun Song,^{es} Jihye Song,^{df} Csaba Soos,^{bc} Francesca Soramel,^{as} Iwona Sputowska,^{dz} Martha Spyropoulou-Stassinaki,^{cz} Brijesh Kumar Srivastava,^{de} Johanna Stachel,^{dd} Ionel Stan,^{bx} Ionel Stan,^{bx} Grzegorz Stefanek,^{dv} Timm Morten Steinbeck,^{bi} Matthew Steinpreis,^{ao} Evert Anders Stenlund,^{bb} Gideon Francois Steyn,^{da} Johannes Hendrik Stiller,^{dd} Diego Stocco,^{dx} Mikhail Stolpovskiy,^{bq} Kirill Strabykin,^{di} Peter Strmen,^{bf} Alexandre Alarcon do Passo Suaide,^{ec} Martin Alfonso Subieta Vasquez,^{ay} Toru Sugitate,^{bl} Christophe Pierre Suire,^{bp} Mikhail Sukhorukov,^{di} Rishat Sultanov,^{bt} Michal Sumbera,^{cu} Tatjana Susa,^{dh} Alejandro Szanto de Toledo,^{ec} Imrich Szarka,^{bf} Adam Szczepankiewicz,^{dz} Artur Krzysztof Szostak,^{an} Maciej Szymanski,^{en} Jun Takahashi,^{ed} Daniel Jesus Tapia Takaki,^{bp} Arturo Tauro,^{bc} Guillermo Tejada Munoz,^{aa} Adriana Telesca,^{bc} Cristina Terrevoli,^{ba} Jochen Mathias Thader,^{dg} Deepa Thomas,^{bs} Raphael Noel Tieulent,^{ee} Anthony Timmins,^{ef} David Tlusty,^{bg} Alberica Toia,^{bi,bc} Hisayuki Torii,^{ei} Luca Toscano,^{dp} David Christopher Truesdale,^{ao} Wladyslaw Henryk Trzaska,^{bk} Tomoya Tsuji,^{ei} Alexandr Tumkin,^{di} Rosario Turrisi,^{do} Trine Spedstad Tvetter,^{aq} Jason Glyndwr Ulery,^{bz} Kjetil Ullaland,^{an} Jochen Ulrich,^{ci,by} Antonio Uras,^{ee} Jozef Urban,^{bh} Guido Marie Urciuoli,^{dq} Gianluca Usai,^{ar} Michal Vajzer,^{bg,cu} Martin Vala,^{cg,bu} Lizardo Valencia Palomo,^{bp} Sara Vallero,^{dd} Naomi van der Kolk,^{ct} Pierre Vande Vyvre,^{bc} Marco van Leeuwen,^{bs} Luigi Vannucci,^{cn} Aurora Diozcora Vargas,^{aa} Raghava Varma,^{bn} Maria Vasileiou,^{cz} Andrey Vasiliev,^{dj} Vladimir Vechernin,^{em} Misha Veldhoen,^{bs} Massimo Venaruzzo,^{at} Ermanno Vercellin,^{ay} Sergio Vergara,^{aa} Renaud Vernet,^{ae} Marta Verweij,^{bs} Linda Vickovic,^{dy} Giuseppe Viesti,^{as} Oleg Vikhlyantsev,^{di} Zabulon Vilakazi,^{da} Orlando Villalobos Baillie,^{dl} Alexander Vinogradov,^{dj} Leonid Vinogradov,^{em} Yury Vinogradov,^{di} Tiziano Virgili,^{ax} Yogendra Viyogi,^{el} Alexander Vodopianov,^{cg} Kirill Voloshin,^{bt} Sergey Voloshin,^{eo} Giacomo Volpe,^{ba,bc} Barthelemy von Haller,^{bc} Danilo Vranic,^{dg} Gaute vrebek,^{an} Janka Vrlakova,^{bh} Bogdan Vulpescu,^{ck} Alexey Vyushin,^{di} Vladimir Wagner,^{bg} Boris Wagner,^{an} Renzhuo Wan,^{cf,bm} Mengliang Wang,^{bm} Dong Wang,^{bm} Yifei Wang,^{dd} Yaping Wang,^{bm} Kengo Watanabe,^{ej} Michael Weber,^{ef} Johannes Wessels,^{bc,cb} Uwe Westerhoff,^{cb} Jens Wiechula,^{ek} Jon Wikne,^{aq} Martin Rudolf Wilde,^{cb} Grzegorz Andrzej Wilk,^{dv} Alexander Wilk,^{cb} Crispin Williams,^{ds} Bernd Stefan Windelband,^{dd} Leonidas Xaplanteris Karampatsos,^{ea} Chris G Yaldo,^{eo} Yorito Yamaguchi,^{ei} Hongyan Yang,^{ak} Shiming Yang,^{an} Stanislav Yasnopolsky,^{dj} JunGyu Yi,^{df} Zhongbao Yin,^{bm} In-Kwon Yoo,^{df} Jongik Yoon,^{es} Weilin Yu,^{bz} Xianbao Yuan,^{bm} Igor Yushmanov,^{dj} Cenek Zach,^{bg} Chiara Zampolli,^{ds} Sergey Zaporozhets,^{cg} Andrey Zarochentsev,^{em} Petr Zavada,^{bw} Nikolai Zaviyalov,^{di} Hanna Paulina Zbroszczyk,^{en} Pierre Zelnicek,^{by} Sorin Ion Zgura,^{bx} Mikhail Zhalov,^{cw} Xiaoming Zhang,^{ck,bm} Haitao Zhang,^{bm} Fengchu Zhou,^{bm} Daicui Zhou,^{bm} You Zhou,^{bs} Jianhui Zhu,^{bm} Jianlin Zhu,^{bm} Xiangrong Zhu,^{bm} Antonino Zichichi,^{au,ai} Alice Zimmermann,^{dd} Gennady Zinovjev,^{ab} Yannick Denis Zoccarato,^{ee} Mykhaylo Zynovyev^{ab} and Maksym Zyzak^{bz}

^{aa} Benemérita Universidad Autónoma de Puebla, Puebla, Mexico

^{ab} Bogolyubov Institute for Theoretical Physics, Kiev, Ukraine

^{ac} Budker Institute for Nuclear Physics, Novosibirsk, Russia

^{ad} California Polytechnic State University, San Luis Obispo, California, United States

^{ae} Centre de Calcul de l'IN2P3, Villeurbanne, France

- ^{af} *Centro de Aplicaciones Tecnológicas y Desarrollo Nuclear (CEADEN), Havana, Cuba*
- ^{ag} *Centro de Investigaciones Energéticas Medioambientales y Tecnológicas (CIEMAT), Madrid, Spain*
- ^{ah} *Centro de Investigación y de Estudios Avanzados (CINVESTAV),
Mexico City and Mérida, Mexico*
- ^{ai} *Centro Fermi – Centro Studi e Ricerche e Museo Storico della Fisica “Enrico Fermi”,
Rome, Italy*
- ^{aj} *Chicago State University, Chicago, United States*
- ^{ak} *Commissariat à l’Energie Atomique, IRFU, Saclay, France*
- ^{al} *Departamento de Física de Partículas and IGFAE, Universidad de Santiago de Compostela, San-
tiago de Compostela, Spain*
- ^{am} *Department of Physics Aligarh Muslim University, Aligarh, India*
- ^{an} *Department of Physics and Technology, University of Bergen, Bergen, Norway*
- ^{ao} *Department of Physics, Ohio State University, Columbus, Ohio, United States*
- ^{ap} *Department of Physics, Sejong University, Seoul, South Korea*
- ^{aq} *Department of Physics, University of Oslo, Oslo, Norway*
- ^{ar} *Dipartimento di Fisica dell’Università and Sezione INFN, Cagliari, Italy*
- ^{as} *Dipartimento di Fisica dell’Università and Sezione INFN, Padova, Italy*
- ^{at} *Dipartimento di Fisica dell’Università and Sezione INFN, Trieste, Italy*
- ^{au} *Dipartimento di Fisica dell’Università and Sezione INFN, Bologna, Italy*
- ^{av} *Dipartimento di Fisica dell’Università ‘La Sapienza’ and Sezione INFN, Rome, Italy*
- ^{aw} *Dipartimento di Fisica e Astronomia dell’Università and Sezione INFN, Catania, Italy*
- ^{ax} *Dipartimento di Fisica ‘E.R. Caianiello’ dell’Università and Gruppo Collegato INFN,
Salerno, Italy*
- ^{ay} *Dipartimento di Fisica Sperimentale dell’Università and Sezione INFN, Turin, Italy*
- ^{az} *Dipartimento di Scienze e Innovazione Tecnologica dell’Università del Piemonte Orientale and
Gruppo Collegato INFN, Alessandria, Italy*
- ^{ba} *Dipartimento Interateneo di Fisica ‘M. Merlin’ and Sezione INFN, Bari, Italy*
- ^{bb} *Division of Experimental High Energy Physics, University of Lund, Lund, Sweden*
- ^{bc} *European Organization for Nuclear Research (CERN), Geneva, Switzerland*
- ^{bd} *Fachhochschule Köln, Köln, Germany*
- ^{be} *Faculty of Engineering, Bergen University College, Bergen, Norway*
- ^{bf} *Faculty of Mathematics, Physics and Informatics, Comenius University, Bratislava, Slovakia*
- ^{bg} *Faculty of Nuclear Sciences and Physical Engineering, Czech Technical University in Prague,
Prague, Czech Republic*
- ^{bh} *Faculty of Science, P.J. Šafárik University, Košice, Slovakia*
- ^{bi} *Frankfurt Institute for Advanced Studies, Johann Wolfgang Goethe-Universität Frankfurt,
Frankfurt, Germany*
- ^{bj} *Gangneung-Wonju National University, Gangneung, South Korea*
- ^{bk} *Helsinki Institute of Physics (HIP) and University of Jyväskylä, Jyväskylä, Finland*
- ^{bl} *Hiroshima University, Hiroshima, Japan*
- ^{bm} *Hua-Zhong Normal University, Wuhan, China*
- ^{bn} *Indian Institute of Technology, Mumbai, India*
- ^{bo} *Indian Institute of Technology Indore (IIT), Indore, India*
- ^{bp} *Institut de Physique Nucléaire d’Orsay (IPNO), Université Paris-Sud, CNRS-IN2P3,
Orsay, France*

- ^{bq}*Institute for High Energy Physics, Protvino, Russia*
- ^{br}*Institute for Nuclear Research, Academy of Sciences, Moscow, Russia*
- ^{bs}*Nikhef, National Institute for Subatomic Physics and Institute for Subatomic Physics of Utrecht University, Utrecht, Netherlands*
- ^{bt}*Institute for Theoretical and Experimental Physics, Moscow, Russia*
- ^{bu}*Institute of Experimental Physics, Slovak Academy of Sciences, Košice, Slovakia*
- ^{bv}*Institute of Physics, Bhubaneswar, India*
- ^{bw}*Institute of Physics, Academy of Sciences of the Czech Republic, Prague, Czech Republic*
- ^{bx}*Institute of Space Sciences (ISS), Bucharest, Romania*
- ^{by}*Institut für Informatik, Johann Wolfgang Goethe-Universität Frankfurt, Frankfurt, Germany*
- ^{bz}*Institut für Kernphysik, Johann Wolfgang Goethe-Universität Frankfurt, Frankfurt, Germany*
- ^{ca}*Institut für Kernphysik, Technische Universität Darmstadt, Darmstadt, Germany*
- ^{cb}*Institut für Kernphysik, Westfälische Wilhelms-Universität Münster, Münster, Germany*
- ^{cc}*Instituto de Ciencias Nucleares, Universidad Nacional Autónoma de México, Mexico City, Mexico*
- ^{cd}*Instituto de Física, Universidad Nacional Autónoma de México, Mexico City, Mexico*
- ^{ce}*Institut of Theoretical Physics, University of Wrocław*
- ^{cf}*Institut Pluridisciplinaire Hubert Curien (IPHC), Université de Strasbourg, CNRS-IN2P3, Strasbourg, France*
- ^{cg}*Joint Institute for Nuclear Research (JINR), Dubna, Russia*
- ^{ch}*KFKI Research Institute for Particle and Nuclear Physics, Hungarian Academy of Sciences, Budapest, Hungary*
- ^{ci}*Kirchhoff-Institut für Physik, Ruprecht-Karls-Universität Heidelberg, Heidelberg, Germany*
- ^{cj}*Korea Institute of Science and Technology Information, Daejeon, South Korea*
- ^{ck}*Laboratoire de Physique Corpusculaire (LPC), Clermont Université, Université Blaise Pascal, CNRS-IN2P3, Clermont-Ferrand, France*
- ^{cl}*Laboratoire de Physique Subatomique et de Cosmologie (LPSC), Université Joseph Fourier, CNRS-IN2P3, Institut Polytechnique de Grenoble, Grenoble, France*
- ^{cm}*Laboratori Nazionali di Frascati, INFN, Frascati, Italy*
- ^{cn}*Laboratori Nazionali di Legnaro, INFN, Legnaro, Italy*
- ^{co}*Lawrence Berkeley National Laboratory, Berkeley, California, United States*
- ^{cp}*Lawrence Livermore National Laboratory, Livermore, California, United States*
- ^{cq}*Moscow Engineering Physics Institute, Moscow, Russia*
- ^{cr}*National Institute for Physics and Nuclear Engineering, Bucharest, Romania*
- ^{cs}*Niels Bohr Institute, University of Copenhagen, Copenhagen, Denmark*
- ^{ct}*Nikhef, National Institute for Subatomic Physics, Amsterdam, Netherlands*
- ^{cw}*Nuclear Physics Institute, Academy of Sciences of the Czech Republic, Řež u Prahy, Czech Republic*
- ^{cv}*Oak Ridge National Laboratory, Oak Ridge, Tennessee, United States*
- ^{cw}*Petersburg Nuclear Physics Institute, Gatchina, Russia*
- ^{cx}*Physics Department, Creighton University, Omaha, Nebraska, United States*
- ^{cyc}*Physics Department, Panjab University, Chandigarh, India*
- ^{cz}*Physics Department, University of Athens, Athens, Greece*
- ^{da}*Physics Department, University of Cape Town, iThemba LABS, Cape Town, South Africa*
- ^{db}*Physics Department, University of Jammu, Jammu, India*

- dc* Physics Department, University of Rajasthan, Jaipur, India
- dd* Physikalisches Institut, Ruprecht-Karls-Universität Heidelberg, Heidelberg, Germany
- de* Purdue University, West Lafayette, Indiana, United States
- df* Pusan National University, Pusan, South Korea
- dg* Research Division and ExtreMe Matter Institute EMMI,
GSI Helmholtzzentrum für Schwerionenforschung, Darmstadt, Germany
- dh* Rudjer Bošković Institute, Zagreb, Croatia
- di* Russian Federal Nuclear Center (VNIIEF), Sarov, Russia
- dj* Russian Research Centre Kurchatov Institute, Moscow, Russia
- dk* Saha Institute of Nuclear Physics, Kolkata, India
- dl* School of Physics and Astronomy, University of Birmingham, Birmingham, United Kingdom
- dm* Sección Física, Departamento de Ciencias, Pontificia Universidad Católica del Perú, Lima, Peru
- dn* Sezione INFN, Trieste, Italy
- do* Sezione INFN, Padova, Italy
- dp* Sezione INFN, Turin, Italy
- dq* Sezione INFN, Rome, Italy
- dr* Sezione INFN, Cagliari, Italy
- ds* Sezione INFN, Bologna, Italy
- dt* Sezione INFN, Bari, Italy
- du* Sezione INFN, Catania, Italy
- dv* Soltan Institute for Nuclear Studies, Warsaw, Poland
- dw* Nuclear Physics Group, STFC Daresbury Laboratory, Daresbury, United Kingdom
- dx* SUBATECH, Ecole des Mines de Nantes, Université de Nantes, CNRS-IN2P3, Nantes, France
- dy* Technical University of Split FESB, Split, Croatia
- dz* The Henryk Niewodniczanski Institute of Nuclear Physics,
Polish Academy of Sciences, Cracow, Poland
- ea* The University of Texas at Austin, Physics Department, Austin, TX, United States
- eb* Universidad Autónoma de Sinaloa, Culiacán, Mexico
- ec* Universidade de São Paulo (USP), São Paulo, Brazil
- ed* Universidade Estadual de Campinas (UNICAMP), Campinas, Brazil
- ee* Université de Lyon, Université Lyon 1, CNRS/IN2P3, IPN-Lyon, Villeurbanne, France
- ef* University of Houston, Houston, Texas, United States
- eg* University of Technology and Austrian Academy of Sciences, Vienna, Austria
- eh* University of Tennessee, Knoxville, Tennessee, United States
- ei* University of Tokyo, Tokyo, Japan
- ej* University of Tsukuba, Tsukuba, Japan
- ek* Eberhard Karls Universität Tübingen, Tübingen, Germany
- el* Variable Energy Cyclotron Centre, Kolkata, India
- em* V. Fock Institute for Physics, St. Petersburg State University, St. Petersburg, Russia
- en* Warsaw University of Technology, Warsaw, Poland
- eo* Wayne State University, Detroit, Michigan, United States
- ep* Yale University, New Haven, Connecticut, United States
- eq* Yerevan Physics Institute, Yerevan, Armenia
- er* Yildiz Technical University, Istanbul, Turkey
- es* Yonsei University, Seoul, South Korea
- et* Zentrum für Technologietransfer und Telekommunikation (ZTT),
Fachhochschule Worms, Worms, Germany